Transport coefficients of He^+ ions in helium

Larry A. Viehland,[1,a)] Rainer Johnsen[2], Benjamin R. Gray[3] and Timothy G. Wright[3]

[1]*Science Department, Chatham University, Pittsburgh, Pennsylvania 15232, USA*

[2]*Department of Physics and Astronomy, University of Pittsburgh, Pittsburgh, Pennsylvania 15260, USA*

[3]*School of Chemistry, University of Nottingham, University Park, Nottingham NG7 2RD, UK*

This paper demonstrates that the transport coefficients of $^4He^+$ in ^4He can be calculated over wide ranges of E/N, the ratio of the electrostatic field strength to the gas number density, with the same level of precision as can be obtained experimentally if sufficiently accurate potential energy curves are available for the $X^2\Sigma_u^+$ and $A^2\Sigma_g^+$ states and one takes into account resonant charge transfer. We start by computing new potential energy curves for these states and testing their accuracy by calculating spectroscopic values for the separate states. It is established that the potentials obtained by extrapolation of results from d-aug-cc-pVXZ (X=6,7) basis sets using the CASSCF+MRCISD approach are each in exceptionally close agreement with the best potentials available and with experiment. The potentials are then used in a new computer program to determine the semi-classical phase shifts and the transport cross sections, and from these the gaseous ion transport coefficients are determined. In addition, new experimental values are reported for the mobilities of $^4He^+$ in ^4He at 298.7 K, as a function of E/N, where careful consideration is given to minimizing various sources of uncertainty. Comparison with previously measured values establishes that only one set of previous data is reliable. Finally, the experimental and theoretical ion transport coefficients are shown to be in very good to excellent agreement, once corrections are applied to account for quantum-mechanical effects.

I. INTRODUCTION

Recent theoretical advances have made it possible to calculate *ab initio* interaction potentials for atomic ion-atom collisions that are highly accurate, and to use the potentials to calculate gaseous ion transport coefficients that meet or exceed the accuracy with which they can be measured[1-4]. Hence gaseous ion transport data serve as stringent tests of the interaction potentials. Advances in the calculation of transport properties, unfortunately, have

a) Author to whom correspondence should be addressed. Electronic mail: viehland@chatham.edu.

not included the situation where atomic ions move through their parent gases, where resonant charge transfer (RCT) can occur. The purpose of this paper is to fill this void.

The occurrence of RCT affects the mobility, diffusion and other transport coefficients that are measured as functions of the gas temperature, T, and the ratio, E/N, of the electrostatic field strength to the gas number density. In particular, when a singly-charged atomic ion collides with a neutral atom of the same kind, an electron can be transferred so that the ion and the neutral interchange roles. The new ion starts its motion through the drift tube as if it were initially at rest, on average, rather than as if it had reached a steady-state average velocity. This means[5] that the ion velocity distribution function along the field is skewed toward small velocities. It will also have kurtoses (coefficients that describe the sharpness of the peak) that are different parallel and perpendicular to the field and it will show correlations between the average speeds and energies in the different directions; these quantities will be discussed more fully below.

It has been known in principle since 1933[6] how to calculate the transport cross sections for systems with RCT from quantum-mechanical phase shifts, and the first numerical values were reported in 1934[7]. These did not agree well with ion mobilities in helium gas at room temperature and low E/N that had finally, just a few years earlier[8], been measured free of the influence of impurities. However, the observed mobilities were shown later[9,10] to correspond to He_2^+ not He^+; RCT means that the lighter, atomic ion moves more slowly through He than does the molecular ion. Progress between the 1930s and the 1960s has been summarized before[11-13]. We will cite more recent work in the appropriate places below.

Although numerical algorithms and computer resources have advanced significantly since the 1960s, it remains difficult to make accurate calculations of transport coefficients when RCT is involved and particularly when the energies probed in drift-tube mass spectrometers are large, arising from high values of T or E/N. This is a result of the large number of phase shifts that are involved, the occurrence of modulo-π errors[14] in the calculation of phase shifts for large angular momentum numbers, and the large number of slightly different transport cross sections that are needed in kinetic theory treatments that describe accurately the experimental values. It is natural then to turn to a semi-classical treatment of the phase shifts.

A semi-classical picture of RCT was given by Holstein[15] in 1952. It indicates that RCT converts a glancing collision into an apparent head-on collision, thus making the energy (ϵ)-dependent, momentum-transfer (or diffusion) cross section, $Q^{(1)}(\epsilon)$, abnormally large compared to the viscosity cross section, $Q^{(2)}(\epsilon)$. In 1958,

Dalgarno[16] gave a semi-classical description of RCT that showed that $Q^{(1)}(\epsilon)$ is approximately twice as large as the cross section for RCT, $Q_{RCT}(\epsilon)$. By 1970, computers had advanced enough that Heiche and Mason[17] could use both quantum-mechanical and semi-classical techniques to calculate $Q_{RCT}(\epsilon)$ and the first three transport cross sections, $Q^{(l)}(\epsilon)$, for He^+ in He. Their results showed that the semi-classical cross sections are quite accurate, particularly when one realizes that it is energy averages of the cross sections that govern the transport coefficients, and that averaging washes out most, but not all, of the structure in the quantum-mechanical cross sections. Sinha et al.[18] showed that the residual differences make the quantum-mechanical mobilities for $^4He^+$ in ^4He at room temperature smaller than the semi-classical values. More recent work is cited at the appropriate places below.

The objectives of this paper are:

1. To obtain potential energy curves for the $X^2\Sigma_u^+$ and $A^2\Sigma_g^+$ states of He_2^+ that merge at large distances onto the ion-induced dipole potential that is known to be asymptotically correct for both states.

2. To show that the spectroscopic quantities computed from the new potentials are in excellent agreement with the available experimental data and with the values computed (separately) from the best previous potentials.

3. To report the development of a new computer program that calculates the semi-classical phase shifts and transport cross sections from a g-u pair of potentials like the ones presented here for He_2^+.

4. To use the cross sections in an existing computer program that determines the mobility and other transport coefficients of $^4He^+$ in ^4He, as functions of T and E/N.

5. To make new measurements of high accuracy of the mobility of $^4He^+$ in ^4He at room temperature as a function of E/N. This is needed because the values obtained by different research groups (cited at the appropriate places below) differ by as much as 7%.

6. To show how the calculated mobilities can be corrected to account for the use of semi-classical rather than quantum-mechanical methods.

7. To show that the corrected mobilities calculated from the new potentials are in excellent agreement with the most reliable experimental data.

II. POTENTIALS

It follows from the assumption of a purely electrostatic Hamiltonian and the Born-Oppenheimer (BO) approximation that different g-u pairs of molecular states do not interact. For He_2^+, the potentials that we are

concerned with are for the $X^2\Sigma_u^+$ and $A^2\Sigma_g^+$ states that are antisymmetric and symmetric, respectively, under exchange of nuclei.

Reagan et al.[19] calculated the $X^2\Sigma_u^+$ potential energy curve (PEC) for He_2^+ for values of the internuclear separation, R, greater than 1.5 bohr, using a 26-term valence-bond function. Browne[20] subsequently calculated the $A^2\Sigma_g^+$ PEC for $R > 1.0$ bohr using a 5-term function; he found strange behavior near 1.5 bohr, which he attributed to an avoided crossing with an even higher excited state. This behavior was also found by Gupta and Matsen[21], who extended the calculations for the $A^2\Sigma_g^+$ PEC down to 0.378 bohr. A reconciliation of these potentials to those calculated in some even earlier work[22] was given by Dickinson[23].

There have been many other calculations of the PECs for He_2^+ over the years[24-32], with the results improving as better algorithms and faster computers became available. Lee[33] reviewed the work up until 1993, and then presented CASSCF+MRCISD calculations (denoted CAS+MRCI hereafter), concluding that the potentials he produced for the $X^2\Sigma_u^+$ and $A^2\Sigma_g^+$ states were reliable and close to what could be expected with full CI calculations; it was acknowledged, however, that the study was limited by the range of basis sets that could be employed.

Following that study, Carrington et al.[34] calculated CAS+MRCI potentials using a range of basis sets, from aug-cc-pVDZ to aug-cc-pV6Z. (For simplicity, we will henceforth refer to these as aVDZ and aV6Z basis sets, making similar abbreviations for other basis sets.) Tests of the potentials against the rovibrational transition energies of Yu and Wing[35] and the almost contemporaneous calculations of Cencek and Rychlewski[36] for the $X^2\Sigma_u^+$ PEC suggested that the potential was producing transition energies that were too low by about 20 cm^{-1}. In Ref. 36, explicitly-correlated Gaussian functions were employed to obtain excellent agreement with the measured infrared (IR) rovibrational transition wave numbers, but it was pointed out[34] that the long-range portion of their $X^2\Sigma_u^+$ potential did not behave satisfactorily. In particular, the energies of the rotational (N) levels for vibrational number $v = 23$ did not give good agreement with the microwave rovibronic transitions.

In 2000, Cencek and Rychlewski[37] reported the lowest variational energy known at the time for He_2^+, and they made estimates of the BO limit of the $X^2\Sigma_u^+$ PEC. Subsequently, Xie et al.[38] used a CAS+MRCI approach together with a daV6Z basis set to calculate BO potentials, along with corrections to the BO approximation. It is stated in that work that the Davidson correction was applied although, as noted by Lee[33] and discussed below, this is inappropriate. Overall, it was found that the calculated transition wave numbers were in better agreement when the

BO-corrected potentials were used, but that the BO potentials seemed to be superior for the IR rovibrational transitions for $v = 0, 1$ in the $X^2\Sigma_u^+$ state and for the microwave rovibronic transitions.

Most recently, Tung et al.[39] published a potential using explicitly-correlated Gaussians and taking adiabatic effects into account. The transition wave numbers they calculated were in excellent agreement with both the microwave[34] and IR[35] measurements.

The best PECs presently available are thus likely to be those in Refs. 38 and 39. Unfortunately, the parameters for the $X^2\Sigma_u^+$ PEC given in the supplementary material for Ref. 38 do not reproduce the well depth given in the text of that paper, so one can only use their $A^2\Sigma_g^+$ potential; additionally, only the $X^2\Sigma_u^+$ PEC was determined by Tung et al.[39]

It is important to note that at large R both PECs should smoothly merge into the ion-induced dipole potential that is shown in Sec. 7-2-A of Mason and McDaniel[40] to vary as $-C_4/R^4$. In atomic units, $C_4 = 0.6918804$ when one uses the value[41] $\alpha = 0.2050522$ Å^3 for the static average electric dipole polarizability of He. The $A^2\Sigma_g^+$ PEC of Xie et al.[38] merges into this so-called polarization potential, but the values of Tung et al.[39] for the $X^2\Sigma_u^+$ PEC for 20.5<R<29.5 bohr lie below the potential of Ref. 38 by amounts that vary erratically from $9.084 - 9.406 \times 10^{-7}$ hartree, with the average deviation being 9.166×10^{-7} hartree. This is most likely because of numerical instability and because the zero of energy, i.e., the value at $R = \infty$, was not set correctly. While this slight error probably does not affect the spectroscopy values reported[39] for the $X^2\Sigma_u^+$ state, it would affect the transport coefficients at low T and E/N. Rather than attempt to modify this $X^2\Sigma_u^+$ potential and then use it with a $A^2\Sigma_g^+$ potential calculated[38] by a different group of researchers using slightly different methods, we decided to compute both potentials again. Another motive for this is that we wished to use "standard" approaches, so that we could assess these for use in calculating the potentials for the heavier diatomic rare gas species, RG_2^+, which will allow the calculation in other papers of the transport properties of RG^+ in RG.

Our strategy is to calculate the potentials for He_2^+ at high levels of theory and to assess these against the spectroscopic data to ascertain their reliability before employing them in transport calculations. All of the calculations were performed using MOLPRO[42,43] with high precision, e.g., the integrals and energies converged within 10^{-12} hartree, which allowed the calculated potentials to extend smoothly out to $R = 150$ Å. For the spectroscopy calculations, we took the energy here to be zero for each PES. For the ion transport calculations, we

merged the calculated potentials with the long-range $-C_4/R_4$ potential, such that all three coincided at this separation; this means that the *ab initio* PECs were decreased by 2.14×10^{-10} hartree (4.70×10^{-5} cm^{-1}) at all R.

Because of the nature of the bonding in He_2^+, it is not possible to identify the fragments unambiguously and carry out full counterpoise corrections for basis set superposition error (BSSE), particularly in the short R region. This was noted by Carrington et al.[34], although they did examine the BSSE, as did Lee[33]. Because of this ambiguity, which risks introducing more errors that it corrects for, and because of the size of our basis sets and the observed convergence of the spectroscopic quantities, including D_e, we are confident that BSSE effects are small in our PECs. (It is noted that Carrington et al. concluded that their uncorrected results seemed to be better than the BSSE-corrected ones.)

One of the most widely-used high-level methods for calculating potentials is the RCCSD(T) method, and so we initially used this with large basis sets, aVXZ (X=Q–7) and daVXZ (X=Q–7), as well as employing pairwise (X^{-3}) extrapolation[44] of the interaction energies. Standard basis sets from the MOLPRO library were employed in all cases except for the following:

(i) The daV6Z basis set was obtained from the standard aV6Z basis set, with the extra sets of diffuse functions being obtained in an even-tempered fashion from the outermost functions.

(ii) The aV7Z and daV7Z basis sets were taken from the literature[45].

However, we found that the long-range behavior was not in agreement with the polarization potential, showing a slight maximum (see below). Therefore, we carried out CAS+MRCI calculations using the molecular orbitals formed from the He 1s, 2s and 2p orbitals. In these calculations, single and double excitations were included but triple excitations (the highest possible excitations for He_2^+) were omitted. To investigate the effect of these omissions and the use of a truncated active space, we then performed a limited set of full CI calculations for the quadruple- and quintuple-ζ basis sets, where we found excellent agreement with the CAS+MRCI results. As discussed below, the CAS+MRCI values obtained by extrapolating d-aug-cc-pVXZ (X = 6, 7) interaction energies represent our most accurate potentials, and they are tabulated in supplementary material.[46]

It should be noted that we did not use the (generalized) Davidson correction to correct for higher-order excitations in the MRCI procedure. This is because, as highlighted by Lee[33], there are only three electrons in He_2^+ while the Davidson correction was designed to correct for quadruple excitations. In addition, the full CI results (see below) indicated that triples contribute only an extremely small amount to the correlation energy.

Fig. 1 shows our values of the PECs of He_2^+ at large separations. At these R values there are still other contributions to the interaction energy; however, our potential steadily approaches agreement with the polarization potential as these other terms die off. It is in excellent agreement with the previous values of Xie et al.[38], but only with those of Tung et al.[39] after their potential is corrected by adding 9.166×10^{-7} hartree, as discussed above.

Fig. 2 shows the present values of the $A^2\Sigma_g^+$ potential of He_2^+ at small separations. Below 1.51 bohr, the present potential shows the unusual behavior reported previously[20,21] and that is assumed to be due to an avoided crossing with a higher excited state at these small R values. This does not appear in the $A^2\Sigma_g^+$ PEC of Xie at al.[38] because that potential was given as a functional form that does not permit such influences to be represented. In calculating spectroscopic quantities, we employ our $A^2\Sigma_g^+$ PEC only for $R > 1.51$ bohr, while for the ion transport calculations we extrapolate to lower separations using an inverse power potential that matches the first two points at R > 1.51 bohr. The potential at small R is so far up on the repulsive wall of the potential that it does not affect the transport calculations at the T and E/N values of interest below.

III. SPECTROSCOPY

From the potentials given in the supplementary material[46], rovibrational energy levels were calculated using Le Roy's LEVEL program[47]. For the $A^2\Sigma_g^+$ state and for the v = 23 level for the $X^2\Sigma_u^+$ state, it was necessary to provide reasonable estimates of the rovibrational energies before convergence was achieved, rather than relying on the default procedure. The final energies of the rovibrational levels were then employed to calculated transition energies that could be compared with experimental results; in addition, spectroscopic quantities were derived and similarly compared.

There are a few key spectroscopic studies to which comparison will be made. In 1995 Carrington et al.[34] recorded rovibronic transitions for He_2^+ between high-lying levels of the $X^2\Sigma_u^+$ state and those of the $A^2\Sigma_g^+$ state; these levels are close enough to allow microwave radiation to effect the transitions. Comparing calculated and experimental values for these transitions allows testing of the high energy region of the $X^2\Sigma_u^+$ state, as well as the potential for the $A^2\Sigma_g^+$ state (which is bound by less than 20 cm^{-1} and only supports two vibrational manifolds and a handful of rotational levels). Prior to this, Yu and Wing[35] had recorded rotationally-resolved IR transitions between the lowest two vibrational levels of the $X^2\Sigma^+$ state of $^3He^4He^+$ (note that the symmetric isotopologues will not be IR active), and so comparison with these transition energies allows some assessment of the $X^2\Sigma_u^+$ PEC close to the

minimum. Pulsed-field ionization zero-kinetic-energy (PFI-ZEKE) spectroscopy via a metastable state of He_2 allowed rotationally-resolved spectra of the lowest three vibrational levels of the $X^2\Sigma_u^+$ state of He_2^+ to be determined[48] for three isotopologues, $^4He_2^+$, $^3He^4He^+$ and $^3He_2^+$. This work has been extended in recent studies[49,50] that allowed the 1–3 and 1–5 rotational spacings in the $X^2\Sigma_u^+$ state of $^4He_2^+$ to be measured very precisely. It should be noted that ^{4}He has a nuclear spin of zero, so it is a boson. As a consequence of this, the odd parity of the $^2\Sigma_u^+$ state with respect to nuclear exchange, and the fact that the vibrational levels are all of positive parity for He_2^+, there are only odd N rotational levels for $^4He_2^+$. It then follows that N=1 is the ground rotational state. This is not true for the $^3He^4He^+$ and $^3He_2^+$ isotopologues, for which all N levels exist, owing to the lack of a center of symmetry for the former and to the alternating degeneracy weighting of 3:1 for the odd:even N levels in the latter.

In Table I we present the vibrational wave numbers for the $X^2\Sigma_u^+$ state of $^4He_2^+$ calculated using RCCSD(T) theory with the aV7Z and daV7Z basis sets. We also present in Table I basis set extrapolated results for the (Q,5), (5,6) and (6,7) pairings, where the extrapolation has been carried out with the X^{-3} scaling of Halkier et al.[44] It may be seen that the differences between the aV7Z and daV7Z results are very small, amounting to < 1 cm^{-1} for each vibrational energy level. It may also be seen from the three pairwise extrapolations that the (5,6) and (6,7) results are very close, with differences of about 0.5 cm^{-1}, while the (Q,5) results are significantly different. Thus convergence with respect to the size of the basis set is close to complete at the quintuple/sextuple-ζ level; also, it seems that a second set of diffuse functions, above that of the "standard" augmentation, is probably not necessary.

In the last two columns of Table I we also give the calculated vibrational energy levels for the isotopologues $^3He^4He^+$ and $^3He_2^+$ using just the (6,7) extrapolated potential. It can be seen that the number of bound vibrational levels decreases as we move from $^4He_2^+$ to $^3He^4He^+$, and again when moving to $^3He_2^+$. (We note that for $^3He^4He^+$ the ground state should be denoted $X^2\Sigma^+$, but we shall always refer to the ground state as the $X^2\Sigma_u^+$ state, since the emphasis in this paper is on ^{4}He; within the BO approximation, these potentials are identical.)

Table I. PEC parameters and vibrational wave numbers in cm^{-1} for the $X^2\Sigma_u^+$ state for the He_2^+ isotopologues, as calculated using RCCSD(T) theory.

			$^4He_2^+$			$^3He^4He^+$	$^3He_2^+$
	aV7Z	daV7Z	(Q,5)[a]	(5,6)[a]	(6,7)[a]	(6,7)[a]	(6,7)[a]
R/Å	1.081	1.081	1.080	1.081	1.081	1.081[b]	1.081[b]
E_{min}/cm^{-1}	-19948.04	-19948.23	-19966.48	-19955.05	-19955.11	-19955.11[b]	-19955.11[b]
v							
0	-19107.65	-19107.85	-19125.67	-19114.37	-19114.55	-19049.16	-18988.32
1	-17479.65	-17479.87	-17496.83	-17485.77	-17486.19	-17298.64	-17124.75
2	-15921.88	-15922.11	-15938.19	-15927.40	-15928.02	-15629.80	-15354.36
3	-14434.42	-14434.68	-14449.81	-14439.39	-14440.16	-14042.80	-13677.34
4	-13017.41	-13017.69	-13031.86	-13021.87	-13022.73	-12537.80	-12093.90
5	-11671.00	-11671.31	-11684.52	-11674.99	-11675.89	-11115.02	-10604.33
6	-10395.37	-10395.72	-10408.04	-10398.94	-10399.86	-9774.73	-9208.98
7	-9190.78	-9191.17	-9202.69	-9193.95	-9194.87	-8517.29	-7908.33
8	-8057.52	-8057.96	-8068.76	-8060.31	-8061.24	-7343.11	-6702.93
9	-6995.96	-6996.46	-7006.61	-6998.40	-6999.33	-6252.73	-5593.50
10	-6006.52	-6007.09	-6016.64	-6008.65	-6009.58	-5246.74	-4580.84
11	-5089.72	-5090.36	-5099.34	-5091.57	-5092.51	-4325.88	-3665.94
12	-4246.16	-4246.87	-4255.29	-4247.77	-4248.70	-3490.98	-2849.95
13	-3476.53	-3477.30	-3485.16	-3477.92	-3478.85	-2743.02	-2134.19
14	-2781.62	-2782.45	-2789.72	-2782.83	-2783.72	-2083.13	-1520.18
15	-2162.33	-2163.20	-2169.86	-2163.39	-2164.22	-1512.55	-1009.60
16	-1619.66	-1620.55	-1626.51	-1620.59	-1621.34	-1032.66	-604.15
17	-1154.69	-1155.58	-1160.70	-1155.52	-1156.15	-644.90	-305.29
18	-768.55	-769.42	-773.52	-769.31	-769.81	-350.48	-113.23
19	-462.33	-463.13	-466.15	-462.98	-463.36	-149.87	-22.47
20	-236.75	-237.43	-239.46	-237.26	-237.54	-40.40	-1.66
21	-91.38	-91.84	-92.96	-91.68	-91.85	-5.07	
22	-20.98	-21.17	-21.58	-21.07	-21.14	-0.003	
23	-2.35	-2.38	-2.44	-2.37	-2.37		

[a] The numbers in parentheses are the cardinal numbers, X, of the daVXZ basis sets, with the corresponding PECs being obtained from an X^{-3} extrapolation.
[b] These are the same as the $^4He_2^+$ values under the BO approximation.

Table II compares the rovibrational wave numbers of Yu and Wing[35] for $^3He^4He^+$ with our calculated wave numbers. As may be seen, the RCCSD(T) (6,7) results are in excellent agreement both with experiment, and also with the results of Tung et al.[39], where the adiabatic effects were concluded as improving significantly the agreement with experiment. It is interesting to note that the RCCSD(T) transition wave numbers are in better agreement with experiment than is the BO potential of Ref. 39, despite their use of explicitly-correlated Gaussian functions; whether

Table II. Calculated versus experimental rovibrational transition wave numbers in cm^{-1} for $^3He^4He^+$.

Transition $v', N' - v'', N''$	Experiment[a] Ref. 35	Present Work RCCSD(T) (6,7)	Present Work CAS+MRCI (6,7)	Previous Work BO[39]	Previous Work BO and Adiabatic[39]	Ref. 36	Ref. 34
1,1 – 0,0		1766.457	1766.363			1766.454	
1,2 – 0,1	1781.839	1781.808	1781.713	1781.867	1781.835	1781.808	1782.072
1,3 – 0,2		1796.557	1796.461			1796.559	1796.821
1,4 – 0,3	1810.717	1810.688	1810.592	1810.749	1810.713	1810.692	1810.951
1,5 – 0,4	1824.212	1824.185	1824.088	1824.245	1824.207	1824.190	1824.446
1,6 – 0,5	1837.055	1837.029	1836.932	1837.090	1837.051	1837.035	1837.287
1,7 – 0,6	1849.229	1849.206	1849.107	1849.267	1849.225	1849.12	1849.460
1,8 – 0,7	1860.719	1860.698	1860.598	1860.759	1860.715	1860.703	1860.948
1,9 – 0,8		1871.489	1871.389			1871.494	1871.733
1,10 – 0,9	1881.580	1881.563	1881.462	1881.623	1881.577	1881.566	1881.801
1,11 – 0,10	1890.916	1890.905	1890.803	1890.964	1890.917	1890.906	1891.135
1,12 – 0,11	1899.509	1899.499	1899.396	1899.556	1899.509	1899.496	1899.720
Deviation[b]		0.016	0.114	0.045	-0.003	0.018	0.227

[a] Only the indicated transitions were observed.
[b] The average deviation of the modulus of the calculated and experimental values.

this is fortuitous or not is difficult to say. We conclude that this ground state BO potential is of a very good quality in the region of the potential minimum and comparable to the best PECs available.

Unfortunately, our RCCSD(T) $X^2\Sigma_u^+$ PEC does not behave as expected close to dissociation. It has a small maximum of about 0.05 cm^{-1} at about $R = 25$ Å. This persists with increased convergence thresholds and seems to be an artifact of the RCCSD(T) method at large R. The result is that the N = 2 level of the v = 23 manifold, the highest vibrational level for which experimental transition have been observed, is not bound and the values for the N = 0 and 1 levels are poor. It is interesting to note that Ref. 39 comments on similarly poor agreement being found for the potential of Cencek and Rychlewski[36].

Because of the poor behavior at large R, CAS+MRCI calculations were performed. We included the He 1s, 2s and 2p orbitals in the active space, and then used the same basis sets and performed the same point-wise extrapolations as for the RCCSD(T) calculations. The calculated vibrational energy levels are presented in Table III for the three extrapolations and for the aV7Z and daV7Z calculations. Additionally, we carried out full CI calculations employing the aVQZ, daVQZ, aV5Z and daV5Z basis sets, and we include the full CI and (Q,5) extrapolated results for the daVXZ basis sets in Table III. The differences in energy levels between full CI (Q,5) and

Table III. CAS+MRCI PEC parameters, and wave numbers (cm^{-1}) for the vibrational energy levels of different isotopologues of He_2^+, relative to the respective dissociation asymptotes.

	$^4He_2^+$						$^3He^4He^+$	$^3He_2^+$
	CAS+MRCI		Full CI	CAS+MRCI	CAS+MRCI	CAS+MRCI		
	aV7Z	daV7Z	(Q,5)[a]	(Q,5)[a]	(5,6)[a]	(6,7)[a]	(6,7)[a]	(6,7)[a]
R/ Å	1.081	1.081	1.080	1.080	1.081	1.081	1.081[b]	1.081[b]
E_{min}/cm^{-1}	-19948.31	-19948.66	-19967.00	-19966.96	-19955.54	-19955.62	-19955.62[b]	-19955.62[b]
v								
0	-19107.96	-19108.32	-19126.24	-19126.20	-19114.90	-19115.11	-19049.71	-18988.88
1	-17480.05	-17480.43	-17497.49	-17497.45	-17486.39	-17486.83	-17299.29	-17125.41
2	-15922.37	-15922.77	-15938.94	-15938.90	-15928.11	-15928.75	-15630.55	-15355.13
3	-14435.02	-14435.44	-14450.66	-14450.63	-14440.19	-14440.98	-14043.65	-13678.21
4	-13018.11	-13018.55	-13032.80	-13032.77	-13022.77	-13023.65	-12538.75	-12094.89
5	-11671.80	-11672.27	-11685.57	-11685.54	-11675.99	-11676.91	-11116.08	-10605.43
6	-10396.28	-10396.79	-10409.20	-10409.17	-10400.04	-10400.98	-9775.91	-9210.21
7	-9191.81	-9192.35	-9203.95	-9203.93	-9195.16	-9196.10	-8518.58	-7909.67
8	-8058.66	-8059.26	-8070.13	-8070.11	-8061.63	-8062.57	-7344.51	-6704.40
9	-6997.21	-6997.86	-7008.07	-7008.06	-6999.82	-7000.76	-6254.24	-5595.08
10	-6007.88	-6008.59	-6018.20	-6018.19	-6010.17	-6011.12	-5248.36	-4582.52
11	-5091.18	-5091.96	-5101.00	-5100.99	-5093.19	-5094.14	-4327.58	-3667.71
12	-4247.72	-4248.56	-4257.03	-4257.02	-4249.47	-4250.41	-3492.76	-2851.77
13	-3478.16	-3479.06	-3486.96	-3486.95	-3479.70	-3480.62	-2744.85	-2136.05
14	-2783.32	-2784.25	-2791.57	-2791.57	-2784.66	-2785.55	-2084.98	-1522.03
15	-2164.07	-2165.03	-2171.73	-2171.73	-2165.24	-2166.07	-1514.39	-1011.38
16	-1621.41	-1622.38	-1628.38	-1628.38	-1622.44	-1623.18	-1034.46	-605.83
17	-1156.41	-1157.38	-1162.52	-1162.53	-1157.33	-1157.96	-646.59	-306.80
18	-770.22	-771.15	-775.27	-775.27	-771.04	-771.54	-352.02	-114.48
19	-463.89	-464.74	-467.77	-467.78	-464.60	-464.98	-151.19	-23.35
20	-238.15	-238.87	-240.90	-240.90	-238.69	-238.98	-41.41	-2.13
21	-92.55	-93.03	-94.17	-94.17	-92.87	-93.04	-5.68	
22	-21.84	-22.03	-22.46	-22.46	-21.93	-22.00	-0.25	
23	-2.85	-2.89	-2.96	-2.96	-2.88	-2.88		

[a] The numbers in parentheses are the cardinal numbers, X, of the (d)aVXZ basis sets, with the corresponding PECs being obtained from an X^{-3} extrapolation (see text).
[b] These are the same as the $^4He_2^+$ values under the Born-Oppenheimer approximation.

CAS+MRCI (Q,5) are extremely small and the transition energy differences will be even smaller, in line with comments made in Ref. 34, and in line with expectations that the contribution from the triple excitations is very minor. Thus, we expect the CAS+MRCI calculations for the larger basis sets to be similarly close to full CI results, and hence the most reliable of these to be the CAS+MRCI (6,7) potentials using the daVXZ basis sets. It is results with this PEC that we use to compare to experiment in more detail.

Table IV. PEC parameters and bound levels (in cm^{-1}) of the $A^2\Sigma_g^+$ state for $^4He_2^+$ calculated using (6,7) basis set extrapolation for the daVXZ basis set.

Level	Ref. 38		Present Work	
	BO	Modified Born	CAS+MRCI	RCCSD(T)
D_e / cm^{-1}	17.3450	17.3820	17.303	16.548
R_e / Å	4.626	4.630	4.616	4.623
v, *N*				
0,0	-8.0944	-8.1182	-8.0261	-7.3851
0,1	-7.4854	-7.5096	-7.4180	-6.7811
0,2	-6.2867	-6.3117	-6.2213	-5.5933
0,3	-4.5410	-4.5668	-4.4791	-3.8662
0,4	-2.3264	-2.3528	-2.2704	-1.6828
1,0	-0.7895	-0.7997	-0.7807	-0.4250
1,1	-0.5568	-0.5664	-0.5488	-0.2105
1,2	-0.1489	-0.1568	-0.1430	unbound
2,0	-0.0003	-0.0005	-0.0003	unbound

For $^4He_2^+$, the 1-3 *N* spacing has been measured[50] as 70.9380±0.0006 cm^{-1} and the 1-5 *N* spacing has been measured[49] as 198.369±0.006 cm^{-1}, each by PFI-ZEKE spectroscopy. Our corresponding calculated spacings are 70.940 cm^{-1} and 198.368 cm^{-1}, so both are in excellent agreement with these very precisely measured experimental values.

Both of our $X^2\Sigma_u^+$ and $A^2\Sigma_g^+$ CAS+MRCI (6,7) potentials go to zero asymptotically, while matching very well the polarization potential discussed above, and this confirms that these are both reliable at large *R* values. We tabulate the bound energy levels of the very weakly-bound $A^2\Sigma_g^+$ state in Table IV. It can be seen that the RCCSD(T) curve, despite performing extremely well close to the minimum (as shown by the close agreement between the calculated and experimental rovibrational levels for the 0–1 transition for the $X^2\Sigma^+$ state of $^3He^4He^+$, discussed above), is not performing as well here, with the (*v*, *N*) = (1,2) and (2,0) levels of the A state not being predicted to be bound. On the other hand, the CAS+MRCI (6,7) curve is performing extremely well, with all bound levels being obtained. We also calculated the wave numbers for the A–X rovibronic transitions and these are compared in Table V both to the experimental values observed by Carrington et al.[34] and to previous calculations. We see that the present potentials are performing exceptionally well – slightly better than even the modified BO potentials of Xie et al.[38]

Table V. Transition wave numbers (in cm^{-1}) for A–X rovibronic transitions for $^4He_2^+$

v'', N'' – v', N'	Expt.[34]	Scaled[a] Ref. 34	Present CAS+ MRCI	Ref. 39 Modified BO	Ref. 39 BO	Ref. 34	Present RCCSD(T)	Ref. 36
23,3–1,2	0.299	0.296	0.286	0.276	0.264	0.243	[b]	[c]
23,1–1,0	1.656	1.652	1.638	1.627	1.594	1.560	1.497	0.926
23,3–0,4	1.864	1.864	1.841	1.920	1.914	1.918	1.669	[c]
23,1–1,2	2.299	2.292	2.275	2.270	2.234	2.199	[b]	1.565
22,5–0,4	3.384	3.384	3.325	3.450	3.439	3.032	3.110	0.615
23,1–0,2	3.821	3.823	3.803	3.885	3.903	3.916	3.672	4.550
23,1–0,0	5.628	5.629	5.608	5.690	5.711	5.721	5.464	6.355
Deviation[d]		0.002	0.025	0.047	0.062	0.121		

[a] These potentials were scaled in Ref. 34 by 1.00128 to match these experimental values.
[b] The 1,2 level of the $A^2\Sigma_g^+$ state is not bound with the calculated potential.
[c] The 23,3 level of the $X^2\Sigma_u^+$ state is not bound with the calculated potential.
[d] Average of the modulus of the difference between the experimental and calculated values.

It is also possible to derive the (23,3)–(22,5) and (23,3)–(23,1) spacings of the $X^2\Sigma_u^+$ state from the microwave transition frequencies (see Fig. 2 of Ref. 39). These values are presented in Table VI where it can be seen that the present $A^2\Sigma_g^+$ potential performs similarly to that of Xie et al.[38], but very slightly poorer than that of Tung et al.[39] (although the differences are all very small, suggesting all three potentials are very reliable in this region.)

Finally, we compare calculated and experimental values for various spectroscopic quantities in Table VII. The level of agreement between the RCCSD(T) and CAS+MRCI potentials is remarkably good throughout. In addition, the agreement with the spectroscopic constants derived from the PFI-ZEKE spectra of Raunhardt et al.[48] is almost always within the experimental error bars, again attesting to the high quality of the present potential, obtained using "standard" methods; we recall that we obtained exceptional agreement with the 1-3 and 1-5 N spacings for more recent PFI-ZEKE results from the same group. The fact that we are making use of the X^{-3} extrapolation of potentials makes this agreement all the more encouraging, particularly since the (5,6) potential appears to be extremely close to that obtained from the more prohibitive (6,7) method; even the (Q,5) potential seems to be "good", but is not at the high level of the other two potentials; additionally, including a second set of diffuse functions makes little difference to the potentials.

Table VI. Wave numbers in cm^{-1} of high-v rovibrational transitions.[b]

	(23,3) → (22,5)	(23,3) → (23,1)
Ref. 39	5.260 (0.012)	2.002 (0.001)
Ref. 38	5.370 (0.122)	1.994 (-0.007)
CAS+MRCI (6,7)	5.166 (-0.082)	1.989 (-0.012)
Experiment[a]	5.248	2.001

[a] Derived from the microwave transition frequencies of Ref. 34 (see Fig II of Ref. 39).
[b] The values in parentheses correspond to the difference (experiment - theory).

Table VII. Spectroscopic parameters for He_2^+ isotopologues. (B_e and α are obtained from B_0 and B_1.)

Quantity	Source	$^4He_2^+$	$^3He^4He^+$	$^3He_2^+$
D_e/ cm^{-1}	RCCSD(T)	19955.11	19955.11	19955.11
	CAS+MRCI	19955.62	19955.62	19955.62
R_e/ Å	RCCSD(T)	1.081	1.081	1.081
	CAS+MRCI	1.081	1.081	1.081
	Expt[48]	1.0806	1.0809	
R_0/ Å	RCCSD(T)	1.0891	1.0898	1.0904
	CAS+MRCI	1.0891	1.0898	1.0904
	Expt[48]	1.08924	1.090	1.0914
ω_e/ cm^{-1}	RCCSD(T)	1698.69	1832.36	1956.92
	CAS+MRCI	1698.61	1832.28	1956.83
	Expt[48]	1698.8	1832.3	1956.9
$\omega_e x_e$/ cm^{-1}	RCCSD(T)	35.16	40.92	46.68
	CAS+MRCI	35.17	40.92	46.68
	Expt[48]	35.18	40.88	46.63
B_e/ cm^{-1}	RCCSD(T)	7.214	8.394	9.574
	CAS+MRCI	7.214	8.394	9.574
	Expt[48]	7.2155	8.393	
B_0/ cm^{-1}	RCCSD(T)	7.1015	8.2526	9.4016
	CAS+MRCI	7.1012	8.2523	9.4012
	Expt[48]	7.1016±0.0005	8.252±0.002	9.388±0.009
B_1/ cm^{-1}	RCCSD(T)	6.8756	7.9689	9.0557
	CAS+MRCI	6.8754	7.9686	9.0553
	Expt[48]	6.8739±0.0005	7.968±0.001	
α/ cm^{-1}	RCCSD(T)	0.22584	0.28369	0.34584
	CAS+MRCI	0.22584	0.28370	0.34585
	Expt[48]	0.2277[a]	0.284[a]	

[a] Obtained from the experimental B_0 and B_1 values.

Our best D_e value is 19955.3 ± 0.3 cm^{-1}, which encompasses both the CAS+MRCI and RCCSD(T) values in Table VII; this value is extremely close to that of Tung et al.[39] who obtained 19954.586 cm^{-1} (from their Table II) or 19956.708 cm^{-1} (from their abstract). Cencek and Rychlewski[37] estimated the exact value for the separated He +

He^+ system to be -4.903724377 hartree; we get -4.903734326 hartree from the correlation energy obtained with the daV6Z and daV7Z basis sets and extrapolated with the X^{-3} formula.

IV. TRANSPORT CROSS SECTIONS

By combining the techniques of Heiche and Mason[17] with the expressions of Wood[51], equations were given by Viehland and Hesche[52] in 1986 for the quantum-mechanical $Q^{(l)}(\epsilon)$ for arbitrary values of l and for a system with RCT. These expressions were given in terms of the phase shifts corresponding to a g-u set of potentials and the wave number for the relative motion of the nuclei. As indicated above, we are interested in the semi-classical expressions, which are obtained by replacing sums over the phase shifts by integrals over the impact parameter, and by approximating the quantum phase shifts.

Two sets of semi-classical equations exist for calculating the transport cross sections. The expressions of Skullerud and Larson[30] are for a set of transport cross sections designated as $q^{(n)}(\epsilon)$, while those of Viehland and Hesche[52] use the $Q^{(l)}(\epsilon)$. The primary difference is that the former involve Legendre polynomials of the cosine of scattering angle while the latter involve powers of the cosine. This is the same kind of difference that arises in different treatments of gaseous ion transport without RCT, and it has been shown[53] that the relationship in that situation is

$$q^{(n)}(\epsilon) = \sum_{l=1}^{n} C(n,l) Q^{(l)}(\epsilon), \tag{1}$$

where

$$C(n,l) = [1 - \{1 + (-1)^l\}/\{2(1+l)\}]^{-1} \sum_{k=l}^{n} (-1)^{k+l} (n+k)!/[2^k k!\,(n-k)!\,l!\,(k-l)!]. \tag{2}$$

We have shown by direct calculation that Eq. (1) is valid for the first four transport cross sections with RCT. The complexity of the semi-classical expressions is such that a rigorous proof for all n seems unlikely. Here we will assume it is true and work only with the expressions in Ref. 52.

A semi-classical computer program named EXCHANGE was developed[52] to compute the transport cross sections for a system with RCT. This program was an improvement on older programs[54-57] in that it was designed to make the necessary numerical integrations to as high an approximation as necessary in order to give $Q^{(l)}(\epsilon)$ values that are at least as precise as the user designates (assuming the potentials are accurate enough to allow this). At that time, precisions of 0.1-1% were considered sufficient.

Since then, improved mathematical techniques have been developed[58] for calculating the $Q^{(l)}(\epsilon)$ with a precision of 0.01% or better in systems without RCT. Because we need high precision in the calculations reported below, we have written a new Fortran computer program called QEx that extends the techniques in Ref. 58 to a g-u pair of potentials for a system with RCT. In the supplementary material[46] we highlight the major aspects of QEx. Copies of the program are available upon request.

As a test of program QEx, we have used it with the "B" potentials of Sinha et al.[18] for He_2^+. The RCT, momentum-transfer and viscosity cross sections we obtained are compared in Fig. 3 with those calculated using program EXCHANGE. The agreement is excellent, but the greater precision obtained with QEx allowed us to determine more carefully the minima in $Q^{(1)}(\epsilon)$ and $Q_{RCT}(\epsilon)$ that occur near 10^{-4} hartree. Note also that the expected result[16] that $Q^{(1)}(\epsilon) \approx 2Q_{RCT}(\epsilon)$ is valid only above thermal energies for this system, as was observed previously[16,59].

V. KINETIC THEORY

Sinha et al.[18] used their potentials to determine the transport cross sections by both quantum-mechanical and semi-classical methods. They then used these cross sections to determine the mobility from the two-temperature (2T) kinetic theory[53,60], which is better than any of the one-temperature (Chapman-Enskog) theories[40,61-63].

The 2T theory starts by assuming that the ion velocity distribution function is approximately Maxwellian (Gaussian), with ion temperatures (average kinetic energies) that are the same along and perpendicular to the electrostatic field but different from the gas temperature. It also assumes in first approximation that there is no skewness, kurtosis or correlation in the distribution function, even though the discussion in the Introduction clearly indicates that RCT should cause such effects. Sinha et al.[18] tried to compensate for these weaknesses by setting the maximum of the ion velocity distribution function equal to a value smaller than the average drift velocity, a procedure that was justified theoretically by Lin and Mason[5]. Nevertheless, their calculated transport properties are unlikely to have the high level of precision desired in the present work.

Two notable advances over the 2T theory are the three-temperature[64,65] (3T) and Gram-Charlier[66] (GC) approaches to solving the Boltzmann equation. The 3T approach is based on a zero-order ion velocity distribution function that has different ion temperatures parallel and perpendicular to the electric field. The GC approach is

based on this same zero-order function multiplied by a set of terms that take into account five other quantities, as follows. The coefficient of skewness along the field is

$$\alpha_L = \langle (v_z - v_d)^3 \rangle / \langle (v_z - v_d)^2 \rangle^{3/2}, \tag{3}$$

where the angle brackets indicate an average over the ion velocity distribution function, the *L* subscript indicates that this is a longitudinal value, parallel to the field, v_z is the longitudinal speed, and v_d is the average drift speed. The kurtoses parallel and perpendicular to the field are

$$\beta_L = \langle (v_z - v_d)^4 \rangle / \langle (v_z - v_d)^2 \rangle^2 \tag{4}$$

and

$$\beta_T = \langle v_x^4 \rangle / \langle v_x^2 \rangle^2, \tag{5}$$

where the *T* subscript indicates that this is a transverse value, perpendicular to the field, and v_x represents the transverse ion speed. (Note that the "excess kurtosis" used by some authors is the kurtosis minus 3.) Finally, the correlation between the perpendicular kinetic energy and the parallel velocity is

$$\gamma_1 = \langle v_x^2 (v_z - v_d) \rangle / \langle v_x^2 \rangle \langle (v_z - v_d)^2 \rangle^{1/2} \tag{6}$$

and the correlation between the perpendicular and parallel kinetic energies is

$$\gamma_2 = \langle v_x^2 (v_z - v_d)^2 \rangle / [\langle v_x^2 \rangle \langle (v_z - v_d)^2 \rangle]. \tag{7}$$

For a Maxwellian (or Gaussian) distribution in three dimensions, $\alpha_L = \gamma_1 = 0$, $\gamma_2 = 1$ and $\beta_T = \beta_L = 3$, so these must be the values at low E/N. In light of the discussion in the Introduction, it is clear that these values will change at intermediate and high E/N. This in turn means that the GC approach should be preferred over the 2T and 3T theories in situations where RCT occurs. As an illustration, we have used the present potentials, program QEx and the GC computer program[67] to determine these quantities for $^4He^+$ in ^4He at 294 K. Fig. 4 compares the results to the values obtained[68] for $^{40}Ca^+$ in ^4He at 300 K; the latter are similar to the results obtained for a large number of ion-neutral systems without RC. The much stronger variation with E/N for $^4He^+$ in ^4He at 294 K is striking.

An enlargement of Fig. 4 at small E/N shows that the distribution starts as a Gaussian at 0 Td, becomes slightly negatively skewed ($\alpha_L < 0$) and platykurtic ($\beta_L < 3, \beta_T < 3$) but still remains almost uncorrelated ($\gamma_1 \approx 0,\ \gamma_1 \approx 0$) near 20 Td, and then returns to being Gaussian near 35 Td. From 35 to 120 Td, Fig. 4 shows that the distribution increasingly becomes more positively skewed, more leptokurtic ($\beta_L > 3, \beta_T > 3$) and more correlated ($\gamma_1 > 0,$ $\gamma_1 > 0$). The tail of a leptokurtic distribution approaches zero more slowly than a Gaussian with the same average velocity. Since the velocity distribution function is normalized, the longer tail and higher peak of a leptokurtic means that it has a smaller width.

VI. QUANTUM EFFECTS

To test program QEx further, we next considered the "4c" potentials of Carrington et al.[34] These potentials were used previously[69] to compute the quantum-mechanical transport cross sections, and these were then used in an early version of the GC computer program to determine the mobilities as a function of E/N at a number of values of T. The precision was estimated to be no worse than 0.1%. We used QEx to calculate the semi-classical cross sections to 0.04% and then used GC to compute the same mobilities with a precision of 0.04%. It was expected[18,30] that the quantum-mechanical values would lie below the semi-classical values, but the differences shown in Fig. 5 allow us to quantify this: quantum-mechanical effects lower the mobilities of $^4He^+$ in ^4He near room temperature by the ratio

$$R_1 = 0.92751424 + 8.3304 \times 10^{-4}(E/N) - 2.40 \times 10^{-6}(E/N)^2, \tag{8}$$

for E/N<180 Td. (There is no difference above 180 Td.) This equation, which assumes that E/N is given in Td, will be used below to correct results calculated for other g-u potentials from QEx and GC. Many of the reasons for doing this rather than making quantum calculations ourselves were given above, but we also note that we are interested in eventually studying the motion of heavier rare gas ions in their parent gases, in which cases the smaller de Broglie wavelengths will allow semi-classical calculations to be used with little or no correction at room temperatures and above. In addition, quantum calculations at low temperatures have already been reported[69], albeit with less accurate potentials than are used here.

Fig. 5 also shows the ratio of the calculated values at 298.7 K to those calculated at 294.0 K. The ratios below 200 Td are described by the equation

$$R_2 = 0.994692 + 5.669 \times 10^{-5}(E/N) - 1.76 \times 10^{-7}(E/N)^2. \quad (9)$$

This equation is in excellent agreement with the temperature dependence of -0.1% per degree suggested in Ref. 70, which implies that $R_2 = 0.9953$ for these two temperatures. Consequently, Eq. (9) will be used below to compare experimental results taken at slightly different temperatures.

To obtain additional information, we considered a pair of potentials for He_2^+ that had been "tuned"[30] to give acceptable agreement with experimental values of the ion mobility. The potentials were tabulated at 22 values of R between 1.3 and 12.0 bohr. (The value at 1.3 bohr of that $A^2\Sigma_g^+$ PEC is in error, presumably because of a misprint, so we removed it.) In order to achieve high precision, we supplemented the tuned potentials by adding eight points at small R (1.08–1.30 bohr), seven points near the minimum of the $A^2\Sigma_g^+$ PEC (8.20–9.75 bohr) and one point at 13.0 bohr. The large-R point was needed to ensure that both potentials matched the correct long-range potential (see above), while the other points were added so that graphs of the potentials were smooth when they were included.

The results obtained from QEx and GC at 294 K with the tuned potentials are compared in Fig. 6 with the experimental values[70] at this temperature and those measured[71] at 295 K. The values at 295 K should be lower than those at 294 K, but they are lower by more than is indicated by Eq. (9). The present semi-classical values have been corrected to the equivalent quantum-mechanical values by using Eq. (8). The corrected values are in excellent agreement with the quantum-mechanical values obtained by Skullerud and Larsen[30] by solving the Boltzmann equation using a single Gaussian weight function, which they found worked only up to 200 Td and hence had to be supplemented at higher E/N by values obtained by computer simulation and by a double Gaussian expansion. What are not in excellent agreement, however, are the differences they reported between their quantum-mechanical and semi-classical mobilities and the ones represented by Eq. (8). Their differences were only half as large as ours, for reasons that must involve their semi-classical calculations. No remarks were made in Ref. 30 about orbiting collisions, multiple orbiting, or the other difficulties outlined in our supplementary material[46]. Accordingly, we believe the present results to be more accurate than the prior semi-classical results for this tuned potential.

VII. EXPERIMENTAL MOBILITIES

Transport coefficients calculated from theoretical interaction potentials can be tested by comparing them to accurate experimental data on gaseous ion mobilities and/or diffusion coefficients. Although it has been shown[72]

that it is better to use diffusion data if both have the same experimental accuracy, mobility values are more easily determined in drift tubes and tend to be more accurate. In a drift-tube experiment one usually infers the ion mobility, K, and the standard (or reduced) ion mobility, K_0, from the average ion speed, often called the drift velocity, using the equations

$$v_d = KE = (NK)(E/N) = (N_0 K_0)(E/N) \tag{10}$$

and

$$v_d = L/\tau\,. \tag{11}$$

Here $N_0 = 2.6867804 \times 10^{25}$ m^{-3} is Loschmidt's constant, L is the length of the drift tube, and τ is the transit time of a short pulse of ions through a gas-filled chamber under the influence of the uniform electrostatic field of magnitude E. Often a mass spectrometer is placed at the exit of the drift tube in order to separate the ion species of interest from others that are formed by reactions with the gas itself, e.g., diatomic molecular ions, or ions arising from reactions with gaseous impurities.

Unfortunately, several complications limit the accuracy of the ion mobilities inferred from the transit time of an ion swarm. The so-called "end effects" arise because the precise position at which a pulse of ions begins to drift with the steady-state velocity, after being produced by an external ion source, is not directly measurable. In addition, if the ions are injected with excess energy they may penetrate a finite distance into the drift space before starting to drift with a steady-state velocity and this can be treated as if the effective length of the drift tube is reduced. Since this is difficult to model, the effective reduction is poorly known. This "injection effect" can be quite large when heavy ions are injected into a light gas like He, but is less important when He^+ ions are injected into helium, because the momentum transfer is strongly enhanced by RCT.

It appears that earlier measurements[8-13,73-84] of the mobilities of $^4He^+$ ions in ^4He were subject to end effects, injection effects and perhaps other complications. This probably accounts for the differences shown in Fig. 6 between the mobilities from Ref. 71 and the other two sets of values. It may also explain why the mobilities measured by Peska[85] were estimated to have fairly large uncertainties, ±6%. The net effect is that the smoothed mobility data given in the compilation by Ellis et al.[86], who took into account the results of several experimental groups, exceed the precise (±0.8-1.5%) values of Helm[70] by more than 7% for E/N>100 Td. We will show below that the values of Helm are undoubtedly the best of the previous experimental values.

In an effort to reduce the uncertainties, we have re-measured the mobility of $^4He^+$ in ^4He using the drift-tube mass spectrometer that at the time was housed at the University of Pittsburgh; it has since been moved to Chatham University. Two different sets of data were taken. The first used the same configuration of the apparatus that was used in earlier measurements[87] of the mobility of O^+ in He. Here, ions generated by a pulsed electron impact ion source are passed through an "injection mass filter" (in actuality, a radio-frequency quadrupole mass filter) before being injected into the drift region through a small orifice. A fraction of the ions that have traversed the drift region is sampled by passing them through a second small orifice and the ions are then mass analyzed by a second quadrupole mass spectrometer and detected by a continuous dynode multiplier. The ion counts are coherently accumulated in a computer-based multichannel analyzer (MCA). The average of the arrival-time distribution must be corrected, in these experiments, for the short time that the ions spend traversing the mass spectrometers. Dividing the drift length by the transit time yields the drift velocity via Eq. (11), and finally Eq. (10) gives the mobility appropriate to the known value of E/N.

The injection mass filter was intended for measurements of ion-molecule reactions but is not really required for mobility studies. It has the disadvantages that it diminishes the ion current and allows the ions to enter the drift tube with energies of 20 to 40 eV; the ensuing injection effect leads to systematic (but variable) errors. A second source of error arises from the non-uniformity of the electric field in the region between the last guard ring and the ion sampling orifice. To overcome these problems, we modified the apparatus by adding two double-grid ion shutters, one located close to the entrance and the other near the end of the drift section (see Fig. 7). We then removed the injection mass filter. The second set of data was collected using this modified drift tube.

The shutter grids, made from very fine nickel gauze, can be electrically biased to either pass or block ions. One grid of each shutter is welded directly to the two plates located at the beginning and end of the drift region, while the other grid is mounted on an insulated ceramic ring. The spacing of the grids in the entrance shutter is slightly smaller (0.176 cm) than those in the exit shutter (0.265 cm). The distance between the two plates that define the beginning and end of the clear drift section is 30.60 cm. This region is enclosed by guard rings that are kept at the appropriate voltages by a resistor chain to make the electric field uniform within 1%; field variations of this magnitude would have a negligible 0.01% effect on the mobility. During measurements, one of the shutters is kept open while the other one is opened only for 2-4 μs by short voltage pulses applied to one of grids. The difference of the arrival times recorded when one or the other shutter is pulsed open reflects the time to traverse the distance

between the two shutters. The spacing of the grids in each shutter, while small, introduces an uncertainty in the distance between the shutters. After some experimentation, we decided that the spacing between the two shutter grids of each shutter should be included in the drift length, increasing its value to $L = 31.04$ cm. This decision contributes an estimated uncertainty of about 0.5% to the measured mobilities.

Even very small blocking voltages (less than 1 V) were found to reduce the transmission of He^+ through the entrance shutter to zero, indicating that these ions lose most of the injection energy in the thermalization region (2 cm long) between the injection orifice and the entrance shutter. Hence there are no injection effects of concern here. Although some heavier ions (e.g. N_2^+, produced from impurities in the ion source) are not completely cut off by the entrance shutter, they have no effect on the He^+ mobility measurements.

The MCA records the arrival time distribution of the He^+ ions arriving during short time windows (channels) of adjustable lengths. The channel width usually was set to 2 μs. The MCA has a built-in program that computes the average of the arrival time distribution, and those averages were usually used in the data analysis. Some sample arrival spectra were examined in greater detail and the MCA averaging routine was found to be accurate. Moreover, we could not detect any skewness or kurtosis in the examined arrival-time distributions.

The spread of arrival times (typically on the order of 10 to 20 μs) was close to, but somewhat larger than, that calculated from the diffusive spread of the spatial ion distribution (see Sec. 1-7 of Ref. 40),

$$\delta_z = \sqrt{\langle (z - z_{max})^2 \rangle} = L(D_L/K)^{1/2} V^{-1/2}. \quad (12)$$

Here δ_z is the average spread of the spatial distribution (in the field direction, z) of the ion cloud and V is the drift voltage. The ratio D_L/K is given as a separate term in Eq. (12) because it is related to the longitudinal ion temperature by a generalized Einstein relation[88] (GER); the values we used are those discussed in Sec. VIII. Eq. (12) was derived for the case where the initial distribution is a delta function along z and where the spread is due to diffusion in the absence of electrostatic repulsion of the ions. The slightly larger spread of the experimental distribution is a consequence of the finite length of the initial ion pulse, not electrostatic repulsion.

A detailed analysis of the shape of the arrival distribution can be found in Sec. 2-2-B of Mason and McDaniel[40]. That analysis includes effects of reactive losses of ions and ion diffusion. The ions that arrive after the average time suffer slightly greater losses than those arriving earlier, and this skews the arrival spectrum. In the case of He^+ ions drifting in He, the dominant reactive loss of He^+ ions is from $He^+ + 2\,He \rightarrow He_2^+ + He$, a very slow ternary reaction with a rate coefficient of 1.1×10^{-31} cm^6 s^{-1} at room temperature[12, 89]. At a helium pressure of 0.5 Torr, thermal

He^+ ions convert to He_2^+ ions with a time constant of 3×10^4 μs, which is much larger than the width of the arrival spectrum. The reaction would change the average arrival time and the inferred mobility by less than 0.001%. Similar estimates indicate that the diffusion effects are equally negligible. This means that that there is little change in the arrival time distribution due to reactions and diffusion.

Sources of He^+ in the drift space can also be excluded. A very small amount of He^{2+} ions are usually observed, but the two-body charge-transfer reaction $He^{2+} + He \rightarrow He^+ + He^+$ is extremely slow, with a thermal rate coefficient[90] of 4.8×10^{-14} cm^3/s. Furthermore, the He^+ product ions arrive at much earlier times than the He^+ ions produced in the source, since the doubly-charged ions have a higher mobility. He^+ products from the He^{2+} reaction have been observed in earlier work[91], but they play no role in the present measurements. Finally, the mass spectrometer's resolution is sufficient to separate He^+ (mass 4) ions from other ions, for instance H_3^+ (mass 3) and HeH^+ (mass 5), that are sometimes present in small amounts; the natural abundance of $^3He^+$ is too low for it to be observed here.

Depending on the desired E/N, the gas pressure in the drift tube was adjusted from 0.16 to 0.62 Torr by a precision leak valve. The helium gas was of ultra-high purity, but small errors (~0.1%) come from the measurement of the gas pressure. The pressures measured by the two Baratron capacitance manometers always agreed to better than 0.1%. The error in the drift voltage is also on the order of 0.1%. The gas temperature was taken as equal to the wall temperature (typically, about 298 K) that was determined by two digital thermometers and one mercury thermometer to an accuracy of 1 K (~0.3%). The uncertainty in the temperature causes a similar fractional error in the gas density that in turn affects E/N and the mobility. The statistical uncertainty in the determination of the average arrival time is on the order of 0.1% or smaller. The time base of the MCA was frequently checked and always found to be accurate. It is concluded that the overall uncertainty of the measured mobilities is not likely to exceed ±1%. The uncertainty in the values of E/N is estimated to be ±0.5%.

The two sets of data taken, one with the original configuration of the drift tube and the other with the shuttered drift tube, do not show a significant difference (see Fig. 8). This was expected because the injection effect discussed earlier is quite small when He^+ ions are injected into helium, because the ions are thermalized rapidly by charge transfer collisions. The advantage of using shutters will be greater in mobility studies of heavier ions in helium.

The present data at T= 298.7 K lie slightly below those of Helm[70] at $T = 294$ K, but Fig. 8 shows that the difference is within the combined error limits when those data are rescaled to 298.7 K by using Eq. (9). Helm's data

were taken in a drift tube that was specifically designed for very accurate mobility measurements and the absence of a mass spectrometer in that apparatus may actually be an advantage for studies of ions drifting in their parent gases. Helm estimated that, at the small helium pressures in his experiments, He_2^+ ions could have contributed an error on the order of only 0.1% to the overall error estimate of 0.8-1.5%, depending upon E/N.

The function given by Patterson[82] is a good representation of all of the data shown in Fig. 8, as well as the earlier data[9,11] from which it was derived. However, it is a bit too high above 50 Td, which is probably a limitation of the functional form that was used and because it was representing data obtained at very high E/N.

The mobility data for $^4He^+$ in ^4He at 300 K taken by Peska[85] lie 1.5 to 2% above those of Helm[70] at 294 K, rather than 0.6% below as one would expect. The drift tube used by Peska included a mass spectrometer and was equipped with shutters similar to those used in the present experiment, and a detailed investigation of the perturbation of the drift field by the shutter potentials was carried out. Although the reason for the large quoted uncertainty (±6%) is not clear, it means that the differences with our results are not statistically significant; because of their large uncertainties, we have chosen not to plot the values from Ref. 85 on Fig. 8.

VIII. ION TEMPERATURES AND DIFFUSION COEFFICIENTS

Before making a direct comparison of the new theoretical and experimental mobilities, we consider the ion temperatures, T_L and T_T, parallel (longitudinal) and perpendicular (transverse), respectively, to the electrostatic field, and then the diffusion coefficients, D_L and D_T.

Applying the GER[88] to systems with RCT, Waldman et al.[92] estimated T_L and T_T for $^4He^+$ in ^4He from the mobilities and diffusion coefficients of Ref. 18. The results were in good agreement with the values obtained by Sinha et al.[30] using a 2T kinetic theory. Unfortunately, both sets of results are based on calculations that started by assuming that T_L and T_T are the same and that the ion velocity distribution function does not show skewness, kurtosis or the correlations that are present in the GC kinetic theory used here. Fig. 9 shows a comparison of our results with those obtained previously. The trends with E/N are consistent, but the previous values are too low for T_T and too high for T_L. This is undoubtedly due to the initial assumptions inherent in the 2T kinetic theory, assumptions that also make the 2T values for D_L and D_T disagree with experiment. Such disagreements were in fact the motivations for developing the 3T[64,65] and GC[66] kinetic theories.

Fig. 10 shows the present results for D_L/K and D_T/K, and compares the latter with the experimental values[93] for $^4He^+$ in ^4He at 294 K. The agreement is good below 50 Td, as was noted in previous papers[69,93] that used different interaction potentials. At higher values, the trends with E/N are consistent but the numerical values are not. Part of the reason is that the present results have not been corrected for quantum-mechanical effects, and these may be larger for the diffusion coefficients than given by Eq. (8) for the ion mobility. However, the differences persist above 200 Td, where quantum effects should be negligible. A second factor is the decreasing precision of our calculated diffusion coefficients as E/N increases. Another factor is the assumption in Ref. 94 that the ions arriving at the collector were "thermalized", i.e. they had suffered enough collisions during their motion through the apparatus that their velocity distribution function had reached steady state. The steady-state assumption is questionable at the low pressure (0.04 Torr) they used to reach E/N values between 400−2000 Td, as the ions would make only 10-12 collisions as they moved through a drift length of 10 cm. Lack of thermalization would make K too large and lead to a value of D_T/K that is too small. A fourth factor is that no detectable deviations from a Gaussian distribution perpendicular to the field were found, even though it had previously been shown by the same authors[94] that such deviations should be expected in even moments of the distribution at high E/N. As noted above, a leptokurtic ion velocity distribution has a smaller width than a Gaussian, which leads to a smaller value of D_T/K. We believe that the last two factors account for most of the difference shown in Fig. 10 between the measured and calculated values of D_T/K above 50 Td.

IX. ION VELOCITY DISTRIBUTION FUNCTIONS

There have been attempts[95-98] to measure the ion velocity distribution by using retarding potentials. The work of Ong and Hogan[99] is particularly relevant to the present paper, since it included figures comparing the velocity distribution functions that were measured for $^4He^+$ in ^4He at room temperature for E/N values between 80 and 242 Td with Gaussian distributions normalized to have the same area. Their results disagree completely with those shown in Figs. 11 and 12 for velocity distributions perpendicular and parallel to the electrostatic field.

Fig. 11 shows how the velocity distribution perpendicular to the field direction changes with increasing E/N. Since increasing E/N causes an increase in the fraction of ions with large velocities, there is consequently a decrease in the fraction of the ions moving perpendicular to the field with small values of v_x. It is also important to

note that this distribution is Gaussian at 0 Td, platykurtic near 10 Td, Gaussian again near 20 Td, and finally becomes strongly leptokurtic as E/N increases above 20 Td.

Fig. 12 compares the calculated velocity distribution parallel to the field to Maxwellian distributions for several values of E/N. It differs significantly from Fig. 11 because increasing E/N causes a shift towards higher speeds along the field direction. Note that even at 86.52 Td this distribution function still has a large fraction of ions moving against the field ($v_z < 0$). This is not a sustained motion, as the distribution function represents the average behavior of the swarm of ions at any particular instant. As a result of collisions that are nearly head-on, some ions will have just bounced off a neutral and be moving against the field at any particular time, until the field slows them and eventually causes them to resume their motion along the field.

The distributions in Fig. 12 are Gaussian at 0 Td, platykurtic at low E/N and strongly leptokurtic at high E/N, just as they are in Fig. 11. We note that the calculated distribution functions are normalized to one over the three-dimensional ion velocity, while the Gaussians in Fig. 12 have the same ion temperatures (distribution widths) as the calculated distributions but are normalized to one over just v_z. This means that the increasing correlations shown in Fig. 4, as well as increasing skewness and kurtosis in the parallel and perpendicular directions, make the calculated distribution at 86.52 Td appear to have a different mean velocity than the Gaussian, even though they are the same.

We believe that the differences between Figs. 11 and 12 and the figures in Ref. 99 arise for three reasons. First, the apparatus used in that work collected all ions coming out of the drift tube within 14 degrees of being on-axis. Second, the authors had no way of correcting for effects caused by the orifice through which the ions were passing before being energy-analyzed. Third, the neutral gas density is reduced near the orifice and the gas flows toward the orifice, thereby "pushing" the ions out in a manner that is difficult to quantify; such effects have been investigated for neutral gases[100,101] but not for ions.

To the best of our knowledge, no attempts have been made since 1985 to measure ion velocity distribution functions with retarding potentials; this is presumably because the experimental problems are so difficult. However, laser-induced fluorescence (LIF) measurements[102-105] of drift-velocity distributions have been able to measure ion temperatures (second moments) and skewness (third moment) that agree well with those calculated from the GER. Unfortunately, very few atomic ions are amenable to single-frequency LIF, and to date measurements have been reported only for Ba^+ in He and Ar.

X. MOBILITY CORRECTIONS

We reported above that the velocity distribution functions at high E/N show large skewness, kurtosis and correlation, and that this accounts, at least partly, for differences between the ion temperatures and diffusion coefficients that we calculated and the limited experimental data that is available. How do they affect the mobility?

Theoretical mobilities are always computed from the average ion velocities, whereas the experimental values reported here, and in most other work, are computed from the length of the drift tube and the average of the ion arrival times. These, and other ways[106,107] of determining the mobility, generally give consistent results when, as reported here, diffusion effects are small and there are no ion-neutral reactions of concern. Indeed, a large number of previous studies[1-4,68] have detected no difference between theoretical and experimental mobilities when the ion-neutral interaction potentials are highly accurate and *ab initio*. However, systems with ion velocity distributions that are highly anisotropic and non-symmetrical, such as those that involve RCT, have not been examined for such differences.

To estimate the effect of the non-Gaussian nature of the ion velocity distribution on the measured mobility, we worked with the transport cross sections determined by program QEx for the present *ab initio* potentials for He_2^+, but we used program GC at 298.7 K in two ways. The first was the standard approach where the calculations started with a Maxwellian distribution at extremely low E/N, and the converged values obtained at one E/N for the ion velocity, ion temperatures and the parameters defined by Eqs. (3)-(7) are used as first approximations for the calculations at a slightly higher E/N; the diffusion coefficients are calculated at each E/N, but are not needed at the next higher value. This approach has the advantage of more rapid convergence at the next value than might otherwise be found, and program GC eventually produces values over a wide range of E/N for the quantities just listed.

The second way we used program GC was to consider only one E/N at a time. We started the program with a Gaussian distribution in which the ion temperature in each direction was set equal to the average ion temperature, $(T_L + 2T_T)/3$, that was calculated with the first method for the same drift velocity. We then allowed GC to calculate the corresponding value of E/N in its first approximation. This value of E/N remained fixed in higher approximations, during which GC modified v_d, T_L, T_T and the five other transport properties. The program stopped when the v_d values were converged to 0.04% or better and the other transport properties to 0.4%.

The first approximation value in the second method of using GC is approximately the combination of v_d and E/N values that correspond to a Gaussian distribution at the average ion temperature. The approximation arises because successive calculations made without changing the zero-order distribution function results, using any kinetic theory, in small changes in the transport properties. For neutral gases, these changes are on the order of 1%, so it is no surprise that in the limit of low E/N we find the ratio of the converged to first-approximation mobility to be 0.99153.

Between 10 and 35 Td, the ratio increased slowly from 0.994 to 1.001. As noted in Sec. V, in this region of E/N the true distribution starts as a Gaussian, becomes slightly skewed (negatively) and slightly platykurtic while remaining almost uncorrelated, and then returns to being Gaussian. From 35 to 120 Td, the ratio decreased monotonically from 1.001 back to 0.994, as the distribution became more positively skewed, more leptokurtic and more correlated. The small changes in the converged mobility are consistent with our finding that the measured arrival time distributions showed no evidence of skewness or kurtosis. Hence no corrections need be applied when comparing our calculated mobilities for systems with RCT to experimental values.

We also considered a possible correction for the fact that the neutral gas used in the experiments was a mixture of the naturally-occurring isotopes of He. We used the average of our two potentials to describe the interaction of $^4He^+$ with ^3He, and combined the cross sections obtained for this potential from program PC[58] with those obtained here with program QEx for $^4He^+$ in ^4He. The abundance of ^3He is so small, however, that the results obtained with program GC[66] are virtually identical with those obtained when the gas was assumed to be completely ^4He. Again, no corrections need be applied.

XI. MOBILITY RESULTS

The solid curve in Fig. 8 represents our best estimate of the experimental mobility of $^4He^+$ in He at 298.7 K. Numerical values are given in Table VIII, where they can be compared with the experimental values of Helm[70], corrected by Eq. (9), and the values calculated from the present potentials and corrected by Eq. (8). The agreement is excellent, given the possible uncertainties in both the experimental and theoretical values.

To demonstrate this quantitatively, we have computed the dimensionless statistical quantities, δ and χ, defined previously[108]. Briefly, δ is a measure of the relative difference between the experimental and calculated values compared to the combined errors, while χ is a measure of the relative standard deviation compared to the sum of the

squared error estimates. We used 1.0% as the maximum inaccuracy for the present data taken with shutters, but we have not taken into account the possible 0.5% errors in the values of E/N. We used the accuracy estimates of Helm[70] for his data at 294 K. For the calculated values we have combined the small convergence errors in QEx and GC and the error associated with using Eq. (8) to estimate a precision of 0.5% below 130 Td, increasing gradually to 1.5% above 500 Td. Finally, we made comparisons at the specific temperatures indicated by the experimenters and we used the raw experimental values.

Table VIII. Mobilities in $cm^2\ V^{-1}\ s^{-1}$ for $^4He^+$ in ^4He at 298.7 K.

E/N (Td)	Present[a]	Ref. 70[b]	Theory[c]
10	10.23	10.35	10.25
15	10.03	10.16	10.12
20	9.83	9.94	9.94
25	9.62	9.70	9.74
30	9.42	9.47	9.53
35	9.22	9.26	9.33
40	9.02	9.04	9.12
60	8.25	8.31	8.38
80	7.59	7.72	7.78
100	7.11	7.23	7.30

[a] Smoothed values obtained from present experimental values taken with shutters.
[b] Converted to 298.7 K with Eq. (9).
[c] Calculated from the present potentials and corrected using Eq. (8).

When the mobilities calculated from the present *ab initio* potentials were compared to the data of Helm[70] at 294 K we obtained $\delta = -0.42$ and $\chi = 0.56$ for the 9 E/N values from 10-80 Td, and $\delta = -0.21$ and $\chi = 1.12$ for all 22 values from 10–1200 Td. For the present experimental values taken with shutters at 298.7 K, we obtained $\delta = -1.34$ and $\chi = 1.49$ for the 21 values between 9.7 and 106 Td. The negative values of δ indicate that the calculated values lie above both sets of experimental mobilities, on the average. Both δ values for the Helm data are below one, so we conclude that there is no statistically significant difference between the experimental and calculated values at 294 K. The δ value for the present data indicates, in contrast, that there is a statistically significant difference at 298.7 K. Note, however, that the values of χ are large enough to indicate that the differences are dependent upon *E*/*N* and/or there are random variations in the raw data used in this analysis. A statistical comparison of the calculated mobilities with the smoothed values at 298.7 K shown in Table VIII gives

$\delta = -1.03$ and $\chi = 1.04$, indicating that the differences may or may not be statistically significant when random fluctuations are eliminated.

Fig. 13 shows graphically that the present calculations are in excellent agreement with the measurements of Helm at 294 and in very good agreement with the present measurements (with shutters) at 298.7 K. The disagreement with the values measured between 130 and 1300 Td by Basurto et al.[109] is substantial. We note, however, that their experiments were conducted between 293 and 310 K with no indication of the temperature of any particular E/N value, and that their values at 130 Td and 200 Td are very close to our calculated values and to Helm's measurements at 294 K. Overall, we believe that the accuracy of the values in Ref. 109 is not as good as the 1.3% that they claimed.

XII. CONCLUSIONS

We have used standard techniques of modern quantum chemistry to determine new potential energy curves for the $X^2\Sigma_u^+$ and $A^2\Sigma_g^+$ states of He_2^+. Although the RCCSD(T) curves show an unphysical maximum at large R, the $X^2\Sigma_u^+$ curve seems to be very accurate close to R_e; the poor behavior close to the asymptote means that the highest levels are not predicted well, and this is also the case for the more weakly-bound $A^2\Sigma_g^+$ state. In contrast the CAS+MRCI curves behave extremely well: at large internuclear distances they merge smoothly onto the polarization potential that is known to be asymptotically correct for both states. We find that the use of basis set extrapolation leads to results that agree extremely closely for both (5,6) and (6,7) extrapolations, and that double augmentation of the basis set makes very little difference. Based on a comparison with experimental spectroscopic results, our best potentials are those calculated by CAS+MRCI with (6,7)-extrapolated daVXZ basis sets. They appear to be as accurate as the best Born-Oppenheimer potentials now available for these states; the best potential for the $X^2\Sigma_u^+$ state is still likely to be the non-BO corrected curve of Tung et al.[39] but even the differences between that potential and ours are extremely small.

We have developed a new computer program, QEx, that calculates the semi-classical phase shifts and transport cross sections from a g-u pair of potentials like the ones presented here for He_2^+. This program allows the user to choose the precision desired, and it has been demonstrated to give results precise within 0.04% or less, which is better than previous programs for systems that allow for RCT.

We have used the *ab initio* cross sections determined by QEx in an existing computer program, GC, to determine the mobility and other transport coefficients of $^4He^+$ in ^4He, as functions of T and E/N. The results at 294 and 298.7 K have been discussed in detail. Similar results at 300, 400 and 500 K have been placed in an on-line database[110]. However, we have not performed calculations at temperatures lower than 294 K because quantum-mechanical effects are expected to dominate over much of the E/N range in such situations.

We have made new measurements of high accuracy of the mobility of $^4He^+$ in ^4He at 298.7 K. These values are in agreement with the best previous data[70], once temperature corrections are applied. The agreement is well within the combined errors (2%). The agreement with the other data[109] available above 130 Td is only within 5%, probably as a result of temperature variations (293–310 K) used in obtaining that data. We conclude that the best available data is that of Helm[70] because he used a drift-tube specifically designed for high accuracy when working with systems with RCT. Our data taken with shutters is a close rival.

It has been shown that two types of corrections must be taken into account before comparing highly precise calculations with highly accurate mobility data. Eq. (8) corrects for the fact that our calculations are entirely semi-classical, whereas the experimental value must of course exhibit quantum-mechanical effects at low energies. Eq. (9) corrects for the fact that even slight temperature differences must be taken into account when one works at the high levels of precision and accuracy used here.

Finally, we have found no statistically-significant differences between our calculations and the data of Helm[70] at 294 K. The differences at 298.7 K with our smoothed data taken with shutters are just on the edge of being statistically significant. These mobility results and the good agreement with spectroscopy values suggest strongly that the *ab initio* potentials, the semi-classical program QEx for determining the transport cross sections, the program GC used to determine the transport coefficients from the cross sections, and the corrections discussed above are all reliable. In future work we intend to study the transport properties of the heavier RG^+ ions in their respective parent gases.

ACKNOWLEDGMENTS

This work was started by Leanne Hindman (nee VanBuren) as part of an undergraduate thesis at Chatham University in 2010. L. A. Viehland is grateful for her interest in the project and for her efforts in demonstrating that the two semi-classical expressions for the transport cross sections are equivalent.

T. G. Wright is grateful for the provision of computing time by the Engineering and Physical Sciences Research Council (EPSRC) under the auspices of the National Service for Computational Chemistry Software (NSCCS), and for access to the University of Nottingham High Performance Computing Facility. Useful conversations with Prof R. J. Le Roy (University of Waterloo) and Prof. F. Merkt (ETH-Zurich) are gratefully acknowledged.

The authors thank Dr. J. de Urquijo for providing a table of the experimental values reported in Ref. 109.

REFERENCES

[1]E. P. F. Lee, L. A. Viehland, R. Johnsen, W. H. Breckenridge and T. G. Wright, J. Phys. Chem. A **115**, 12126 (2011).

[2]A. A. Buchachenko and L. A. Viehland, J. Chem. Phys. **140**, 114309 (2014).

[3]W. D. Tuttle, R. L. Thorington, L. A. Viehland and T. G. Wright, Molec. Phys. **113**, 3767 (2015).

[4]L. A. Viehland and C.-L. Yang, Molec. Phys., on-line publication August 21, 2015. DOI: 10.1080/00268976.2015.1074746.

[5]S. L. Lin and E. A. Mason, J. Phys. B **12**, 783 (1979).

[6]H. S. W. Massey and R. A. Smith, Proc. Roy. Soc. (London) A **142**, 142 (1933).

[7]H. S. W. Massey and C. B. O. Mohr, Proc. Roy. Soc. (London) A **144**, 188 (1934).

[8]A. M. Tyndall and C. F. Powell, Proc. Roy. Soc. (London) A **134**, 125 (1931).

[9]J. A. Hornbeck, Phys. Rev. **84**, 615 (1951).

[10]A. V. Phelps and S. C. Brown, Phys. Rev. **86**, 102 (1952).

[11]E. C. Beaty and P. L. Patterson, Phys. Rev. A **37**, 346 (1965).

[12]J. M. Madson, H. J. Oskam and L. M. Chanin, Phys. Rev. Lett. **15**, 1018 (1965).

[13]O. J. Orient, Can. J. Phys. **45**, 4015 (1967).

[14]H. Wei and R. J. Le Roy, Molec. Phys. **104**, 147 (2006).

[15]T. Holstein, J. Phys. Chem. **56**, 832 (1952).

[16]A. Dalgarno, Phil. Trans. Roy. Soc. A **250**, 426 (1958).

[17]G. Heiche and E. A. Mason, J. Chem. Phys. **53**, 4687 (1970).

[18]S. Sinha, S. L. Lin and J. N. Bardsley, J. Phys. B **12**, 1613 (1979).

[19]P. N. Reagan, J. C. Browne and F. A. Matsen, Phys. Rev. **132**, 304 (1963).

[20]J. C. Browne, J. Chem. Phys. **45**, 2707 (1966).

[21]B. K. Gupta and F. A. Matsen, J. Chem. Phys. **47**, 4860 (1967).

[22]S. Weinbaum, J. Chem. Phys. **3**, 574 (1935).

[23]A. S. Dickinson, J. Phys B. **1**, 387 (1968).

[24]R. J. Damburg and R. Kh. Propin, J. Phys. B. **1**, 681 (1968).

[25]D. R. Bates and R. H. G. Reid, Adv. At. Mol. Phys. **4**, 13 (1968).

[26]B. Liu, Phys. Rev. Lett. **27**, 1251 (1971).

[27]J. G. Maas, N. P. F. B. van Asselt, P. J. C. M. Nowak, J. Los, S. D. Peyerimhoff and R. J. Beunker, Chem. Phys. **17**, 217 (1976).

[28]A. Metropoulos, C. A. Nicolaides and R. J. Buenker, Chem. Phys. **114**, 1 (1987).

[29]C. W. Bauschlicher Jr., H. Partridge and D. Ceperley, Chem. Phys. Lett. **160**, 183 (1989).

[30]H. R. Skullerud and P.-H. Larsen, J. Phys. B. **23**, 1017 (1990).

[31]J. Ackermann and H. Hogreve, Chem. Phys. **157**, 75 (1991).

[32]A. Metropoulos, Y. Li, G. Hirsch and R. J. Buenker, Chem. Phys. Lett. **92**, 266 (1992).

[33]E. P. F. Lee, J. Chem. Soc. Faraday Trans. **89**, 645 (1993).

[34]A. Carrington, C. H. Pyne and P. J. Knowles, J. Chem. Phys. **102**, 5979 (1995).

[35]N. Yu and W. H. Wing, Phys. Rev. Lett. **59**, 2055 (1987).

[36]W. Cencek and J. Rychlewski, J. Chem. Phys. **102**, 2533 (1995).

[37]W. Cencek and J. Rychlewski, Chem. Phys. Lett. **320**, 549 (2000).

[38]J. Xie, B. Poirier and G. I. Gellene, J. Chem. Phys. **122**, 184310 (2005).

[39]W.-C. Tung, M. Pavanello and L. Adamowicz, J. Chem. Phys. **136**, 104309 (2012).

[40]E. A. Mason and E. W. McDaniel, *Transport Properties of Ions in Gases* (Wiley, N.Y., 1988).

[41]J. W. Schmidt, R. M. Glavioso. E. F. May and M. R. Moldover, Phys. Rev. Lett. **98**, 254504 (2007).

[42]MOLPRO is a package of *ab initio* programs written by H.-J. Werner, P.J. Knowles, G. Knizia, F.R. Manby, M. Schütz, P. Celani, T. Korona, R. Lindh, A. Mitrushenkov, G. Rauhut, K.R. Shamasundar, T.B. Adler, R.D. Amos, A. Bernhardsson, A. Berning, D.L. Cooper, M.J.O. Deegan, A.J. Dobbyn, F. Eckert, E. Goll, C. Hampel, A.

Hesselmann, G. Hetzer, T. Hrenar, G. Jansen, C. Köppl, Y. Liu, A.W. Lloyd, R.A. Mata, A.J. May, S.J. McNicholas, W. Meyer, M.E. Mura, A. Nicklaß, D.P. O'Neill, P. Palmieri, D. Peng, K. Pflüger, R. Pitzer, M. Reiher, T. Shiozaki, H. Stoll, A.J. Stone, R. Tarroni, T. Thorsteinsson, M. Wang.

[43]H.-J. Werner, P. J. Knowles, G. Knizia, F.R. Manby and M. Schütz, WIREs Comput. Mol. Sci. **2**, 242 (2012).

[44]A. Halkier, T. Helgaker, P. Jørgensen, W. Klopper, H. Koch, J. Olsen and A. K. Wilson, Chem. Phys. Lett. **286**, 243 (1998).

[45]R. Hellmann, E. Bich and E. Vogel, Molec. Phys. **105**, 3013 (2007).

[46]See supplementary material at http://dx.doi.org/10.1063/ .

[47]R. J. Le Roy, *Level 8.2: A Computer Program for Solving the Radial Schrodinger Equation for Bound and Quasibound Levels* (University of Waterloo Chemical Physics Research Report CP-668, 2014).

[48]M. Raunhardt, M. Schäfer, N. Vanhaecke and F. Merkt, J. Chem. Phys. **128**, 164310 (2008).

[49]D. Sprecher, J. Liu, T. Krähenmann, M. Schäfer and F. Merkt, J. Chem. Phys. **140**, 064304 (2014).

[50]P. Jansen, L. Semeria, L. E. Hofer, S. Scheidegger, J. A. Agner, H. Schmutz and F. Merkt, Phys. Rev. Lett. **115**, 133202 (2015).

[51]H. T. Wood, J. Chem. Phys. **54**, 977 (1971).

[52]L. A. Viehland and M. Hesche, Chem. Phys. **110**, 41 (1986).

[53]L. A. Viehland and E. A. Mason, Ann. Phys. (N.Y.) **110**, 287 (1978).

[54]R. J. Munn, E. A. Mason and F. J. Smith, J. Chem. Phys. **41**, 3978 (1964).

[55]R. R. Herm, J. Chem. Phys. **47**, 4290 (1967).

[56]W. H. Miller, J. Chem. Phys. **48**, 1651 (1968).

[57]J. N. L. Connor, Molec. Phys. **23**, 717 (1972).

[58]L. A. Viehland and Y. Chang, Comp. Phys. Commun. **181**, 1687 (2010).

[59]N. Lynn and B. L. Moiseiwitsch, Proc. Phys. Soc. A **70**, 474 (1957).

[60]L. A. Viehland and E. A. Mason, Ann. Phys. (N.Y.) **91**, 499 (1975).

[61]Yu. P. Mordvinov and B. M. Smirnov, Sov. Phys. JETP **21**, 91 (1965).

[62]B. M. Smirnov, Sov. Phys. Uspekhi **10**, 313 (1967).

[63]T. Dote and M. Shimada, J. Phys. Soc. Japan **50**, 1608 (1981).

[64]S. L. Lin, L. A. Viehland and E. A. Mason, Chem. Phys. **37**, 411 (1979).

[65]L. A. Viehland and S. L. Lin, Chem. Phys. **43**, 135 (1979).

[66]L. A. Viehland, Chem. Phys. **179**, 71 (1994).

[67]A. Yousef, S. Shrestha, L. A. Viehland, E. P. F. Lee, B. R. Gray, V. L. Ayles, T. G. Wright and W. H. Breckenridge, J. Chem. Phys. **127**, 154309 (2007).

[68]A. M. Gardner, C. D. Withers, T. G. Wright, K. I. Kaplan, C. Y. N. Chapman, L. A. Viehland, E. P. F. Lee and W. H. Breckenridge, J. Chem. Phys. **132**, 054302 (2010).

[69]A. S. Dickinson, M. S. Lee and L. A. Viehland, J. Phys. B **32**, 4919 (1999).

[70]H. Helm, J. Phys. B **10**, 3683 (1977).

[71]R. Johnsen, M. T. Leu and M. A. Biondi, Phys. Rev. A **8**, 2557 (1973).

[72]M. J. Hogan, J. Chem. Phys. **125**, 164325 (2006).

[73]A. M. Tyndall and C. F. Powell, Proc. Roy. Soc. A **129**, 162 (1930).

[74]A. M. Tyndall and A. F. Pearce, Proc. Roy. Soc. A **149**, 426 (1935).

[75]M. A. Biondi and S. C. Brown, Phys. Rev. **75**, 1700 (1949).

[76]M. A. Biondi and L. M. Chanin, Phys. Rev. **94**, 910 (1954).

[77]L. M. Chanin and M. A. Biondi, Phys. Rev. **106**, 473 (1957).

[78]H. J. Oskam and V. R. Mittelstadt, Phys. Rev. **132**, 1435 (1963).

[79]R. Hackam and J. J. Lennon, Proc. Phys. Soc. **84**, 133 (1964).

[80]E. C. Beaty, J. C. Browne and A. Dalgarno, Phys. Rev. Lett. **16**, 723 (1966).

[81]P. L. Patterson, J. Chem. Phys. **48**, 3625 (1968).

[82]P. L. Patterson, Phys. Rev. A **2**, 1154 (1970).

[83]R. A. Gerber and M. A. Gusinow, Phys. Rev. A **4**, 2027 (1971).

[84]B. L. Henson, Phys. Rev. A **15**, 1680 (1977).

[85]N. Peska. Dissertation. Leopold-Franzens-Universität, 1981.

[86]H. W. Ellis, R. Y. Pai, E. W. McDaniel, E. A. Mason and L. A. Viehland, At. Data Nucl. Data Tables **17**, 177 (1976).

[87]D. M. Danailov, L.A. Viehland, R. Johnsen, T.G. Wright and A.S. Dickinson. J. Chem. Phys. **128**, 134302 (2008).

[88]M. Waldman and E. A. Mason, Chem. Phys. **58**, 121 (1981).

[89]R. Johnsen, A. Chen and M. A. Biondi, J. Chem. Phys **73**, 1717 (1981).

[90]R. Johnsen and M. A. Biondi, Phys. Rev. A **20**, 87 (1979).

[91]R. Johnsen and M. A. Biondi, Phys. Rev. A **18**, 996 (1978).

[92]M Waldman, E. A. Mason and L. A. Viehland, Chem. Phys. **66**, 339 (1982).

[93]T. Stefánsson, T. Berge, R. Lausund and H. R. Skullerud, J. Phys. D **21**, 1359 (1988).

[94]H. R. Skullerud, T. Eide and T. Stefánsson, J. Phys. D **19**, 197 (1986).

[95]J. L. Moruzzi and L. Harrison, Int. J. Mass Spectrom. Ion Phys. **13**, 163 (1974).

[96]K. Naveed-Ullah, D. Mathur and J. B. Hasted, Int. J. Mass Spectrom. Ion Phys. **26**, 91 (1978).

[97]P. P. Ong, D. Mathur, M. H. Khatri, J. B. Hasted and M. Hamdan, J. Phys. D **14**, 633 (1981).

[98]H. A. Fhadil, D. Mathur and J. B. Hasted, J. Phys. B **15**, 1443 (1982).

[99]P. P. Ong and M. J. Hogan, J. Phys. B **18**, 1897 (1985).

[100]C. Cercignani and F. Sharipov, Phys. Fluids A **4**, 1283 (1992).

[101]R. Johnsen and B. K. Chatterjee, J. Vac. Sci. Technol. A **29**, 011002 (2011).

[102]R. A. Dressler, H. Meyer, A. O. Langford, V. M. Bierbaum and S. R. Leone, J. Chem. Phys. **87**, 5578 (1987).

[103]R. A. Dressler, J. P. M. Beijers, H. Meyer, S. M. Penn, V. M. Bierbaum and S. R. Leone, J. Chem. Phys. **89**, 4707 (1988)

[104]S. M. Penn, J. P. M. Beijers, R. A. Dressler, V. M. Bierbaum and S. R. Leone, J. Chem. Phys. **93**, 5118 (1990).

[105]M. J. Bastian, C. P. Lauenstein, V. M. Bierbaum and S. R. Leone, J. Chem. Phys. **98**, 9496 (1993).

[106]H. Tagashira, Y. Sakai and S. Sakamoto, J. Phys. D **10**, 1051 (1977).

[107]K. Kondo and H. Tagashira, J. Phys. D **23**, 1175 (1990).

[108]L. A. Viehland, Chem. Phys. **85**, 291 (1984).

[109]E. Basurto, J. de Urquijo, I. Alvarez and C. Cisneros, Phys. Rev. E **61**, 3053 (2000).

[110]www.icecat.laplace.univ-tlse.fr

Figure Captions

Fig. 1. Potential energy (V in hartree) as a function of the internuclear separation (R in bohr) for He_2^+, at large R. The blue diamonds are the present values for the $X^2\Sigma_u^+$state, the superimposed, small orange circles are for the $A^2\Sigma_g^+$ state, and the light green triangles are the polarization potential. The solid red curve shows the values of Tung et al.[39] for the $X^2\Sigma_u^+$state, while the dashed red curve was obtained by correcting the values of Ref. 39 in the manner discussed in the text. The dotted blue curve shows the values of Xie et al.[38] for the $A^2\Sigma_g^+$ state.

Fig. 2. Potential energy (V in hartree) as a function of the internuclear separation (R in bohr) for the $A^2\Sigma_g^+$ state of He_2^+ at small R. The blue circles are the present values and the solid red curve shows the values of Xie et al.[38]

Fig. 3. Collision frequencies, υ in atomic units, for $^4He^+$ ions moving through ^4He gas, as a function of the collision energy, ε in hartree. The blue circles connected by a blue curve are the momentum-transfer collision frequencies, $\upsilon^{(1)}(\varepsilon) = \sqrt{\varepsilon}Q^{(1)}(\varepsilon)$, calculated from the potentials of Sinha et al.[18] using program QEx and having a precision of 0.04%. The red circles are the viscosity collision frequencies, $\upsilon^{(2)}(\varepsilon) = \sqrt{\varepsilon}Q^{(2)}(\varepsilon)$, calculated in the same way. The small black points were calculated previously[52] from the same potentials but using program EXCHANGE and having a precision of 0.2%. The dashed blue curve represents twice the value of the collision frequency for RCT, i.e. $2\sqrt{\varepsilon}Q_{RCT}(\varepsilon)$.

Fig. 4. The dimensionless quantities defined by Eqs. 3-7, as a function of E/N in Td. The solid curves are based on the present potentials for $^4He^+$ in ^4He at 294 K. The dashed curves are for $^{40}Ca^+$ in ^4He at 300 K and are calculated from the potential in Ref. 68; they show typical results for a system without RCT.

Fig. 5. Ratio, R_1, of the quantum-mechanical mobilities to the semi-classical values for $^4He^+$ in ^4He at 294 K, and ratio, R_2, of the calculated mobilities at 298.7 K to those at 294.0 K. The circles were obtained from the calculations discussed in the text. The curves are obtained from Eqs. (8) and (9).

Fig. 6. Mobilities, K_0 in $cm^2\,V^{-1}\,s^{-1}$, as a function of the reduced field strength, E/N in Td, for $^4He^+$ ions in ^4He gas at 294 K. Programs QEx and GC were used to calculate the semi-classical mobilities from the potentials of Skullerud and Larsen[30]. The dark blue points at low E/N were calculated with a precision of 0.04%, the blue points at intermediate E/N with a precision of 0.5%, and the light blue points at high E/N are precise with 1.0%. The blue curve was obtained by correcting the calculated values to equivalent quantum-mechanical mobilities, using Eq. (8). The black points with small error bars are the experimental values of Helm[70], while those with larger error bars are the values (at 295 K) of Johnsen et al.[71]

Fig. 7. Schematic diagram of the Pittsburgh drift-tube mass spectrometer, modified as described in the text.

Fig. 8. Comparison of the present mobility data for $^4He^+$ in ^4He with selected earlier experimental data. The dark blue circles are the present data taken without shutters; they are generally below the light blue circles that represent data taken with shutters. The solid curve is a polynomial fit to the shuttered data and represents our best estimate of our mobilities. The red circles that lie slightly above the curve are the data of Helm[70] scaled by Eq. (9) to compensate for the difference in temperatures. The dashed purple line represents the function of Patterson[82] for mobilities at 300 K, divided by 0.9987 to correspond to 298.7 K.

Fig. 9. Ion temperatures, T_L and T_T in K, for $^4He^+$ in ^4He at 294 K. The red squares were calculated by Sinha et al.[18] and the blue circles by Waldman et al.[92] The curves are the present values.

Fig. 10. The ratios, D_L/K and D_T/K in mV, of the diffusion coefficients parallel and perpendicular to the electrostatic field to the mobilities, for $^4He^+$ in ^4He at 294 K as a function of E/N in Td. The black points with error bars are the experimental values[93] for D_T/K and the black curve represents the smoothed values[94]. The other points show the present values; possible convergence errors of the dark blue points at small E/N are no more than 0.4%, the blue values 1%, the light blue values 1.5%, the green values 4% and the red values 10%.

Fig. 11. Ion speed distribution function perpendicular to the field, f_x, for $^4He^+$ in ^4He at 294 K, as a function of the ion speed, v_x in m/s, and when normalized to one when integrated over all velocities, not just v_x. The curves are calculated from the present potentials and the squares represent a Gaussian (normal) distribution. From top to bottom, the dark blue curve and points are for *E*/*N*=0.15 Td, the blue ones are for 9.89 Td, the light blue for 20.13 Td, the green for 31.65 Td, the light green for 52.25 Td, and the red ones for 86.52 Td.

Fig. 12. Ion speed distribution function parallel to the field, f_z, for $^4He^+$ in ^4He at 294 K, as a function of the ion speed, v_z in m/s, and when normalized to one when integrated over all velocities, not just v_z. The curves are calculated from the present potentials and the squares represent a Gaussian (normal) distribution. From left to right, the dark blue curve and points are for *E*/*N*=0.15 Td, the light blue ones are for 20.13 Td, the green for 31.65 Td, the light green for 52.25 Td, and the red ones for 86.52 Td.

Fig. 13. Standard mobilities, K_0 in $cm^2\ V^{-1}\ s^{-1}$, as a function of the reduced field strength, E/N in Td, for $^4He^+$ in He. The black, upper points with error bars are the values of Helm[70], the blue, lower points below 100 Td are the present values at 298.7 K, and the purple, lowest points above 130 Td are the values of Basurto et al.[109] at 297-310 K. The black, top curve was calculated from the present potentials at 294 K and corrected with Eq. (8). The blue, lower curve below 200 Td was calculated similarly at 298.7 K. The violet, lowest curve above 130 Td represents the function given in Ref. 109.

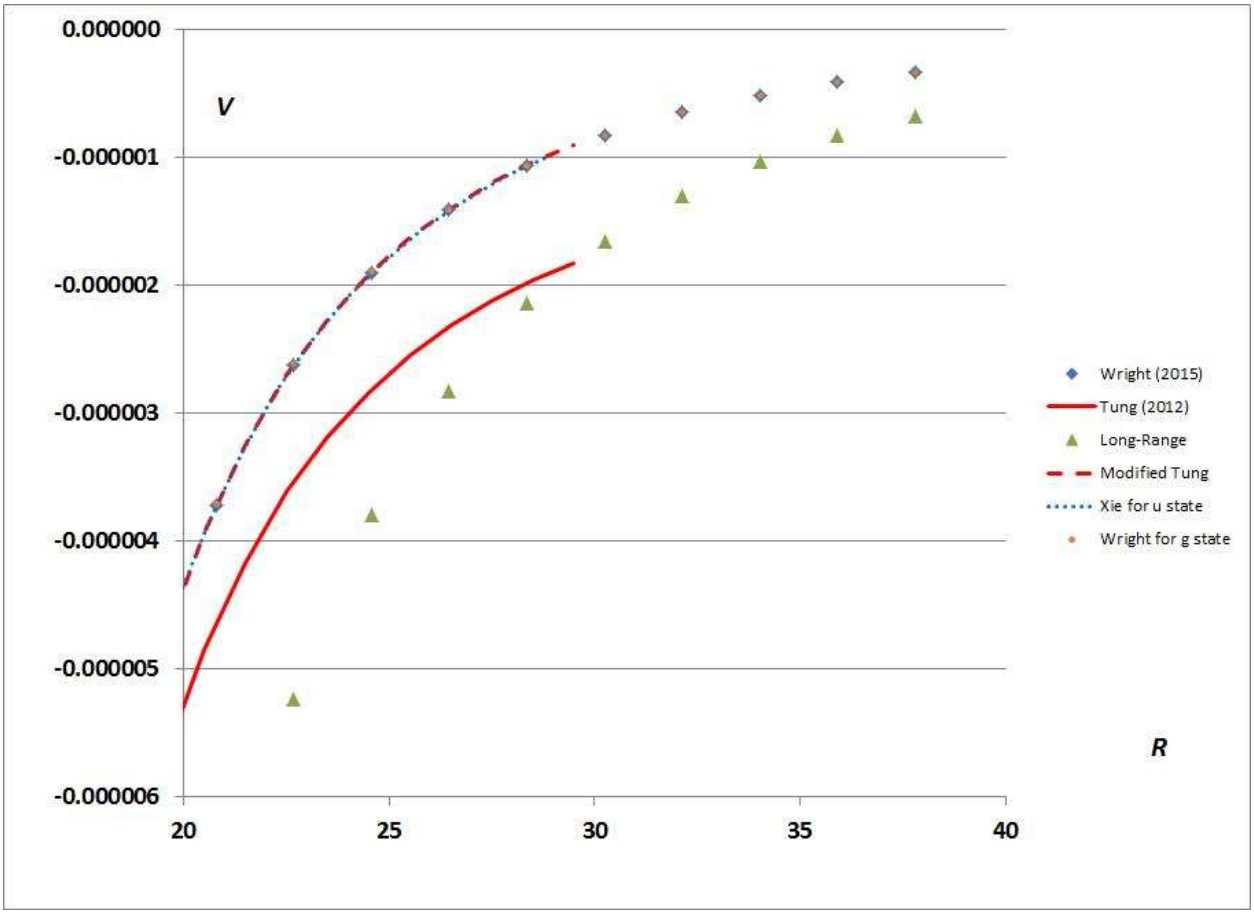

Fig. 1 of Viehland et al.

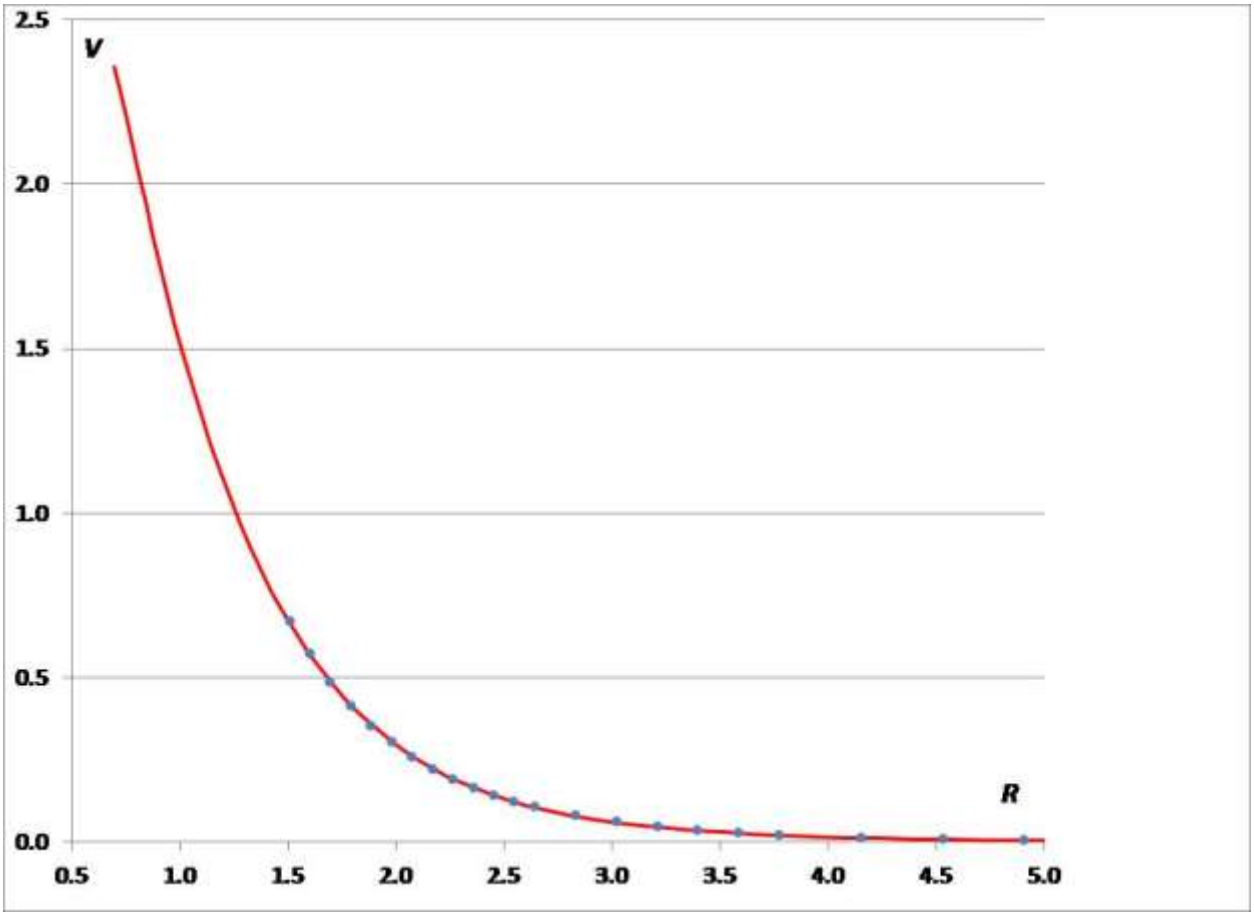

Fig. 2 of Viehland et al.

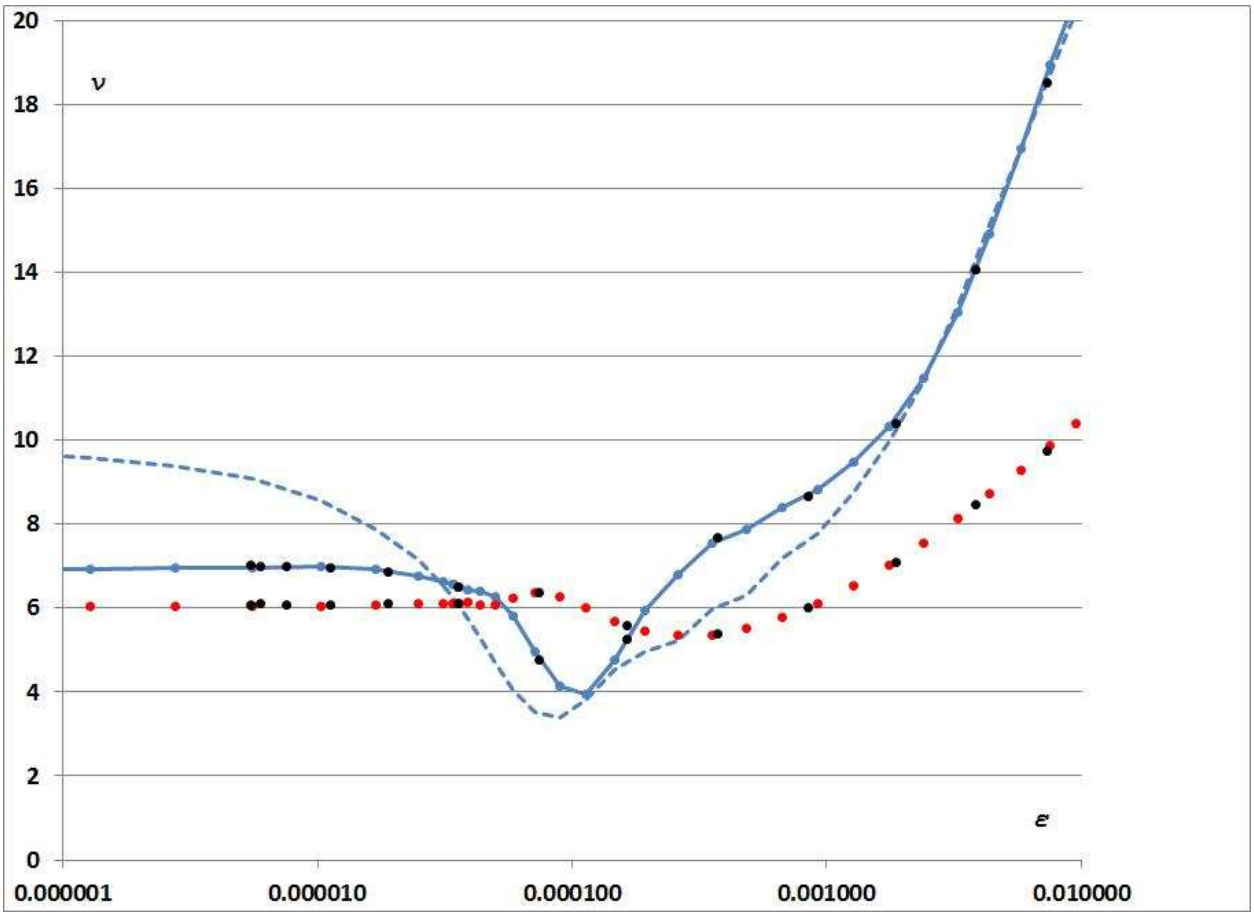

Fig. 3 of Viehland et al.

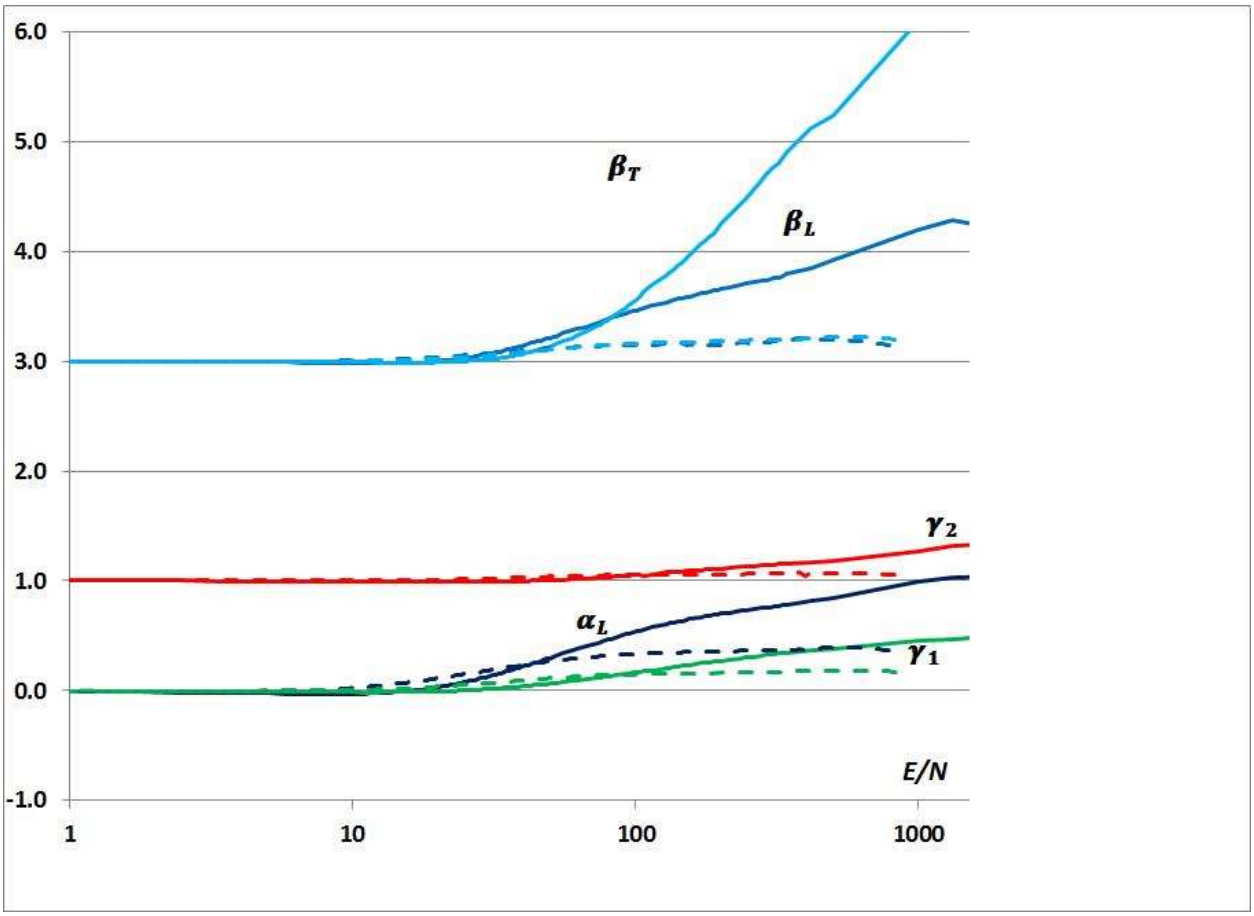

Fig. 4 of Viehland et al.

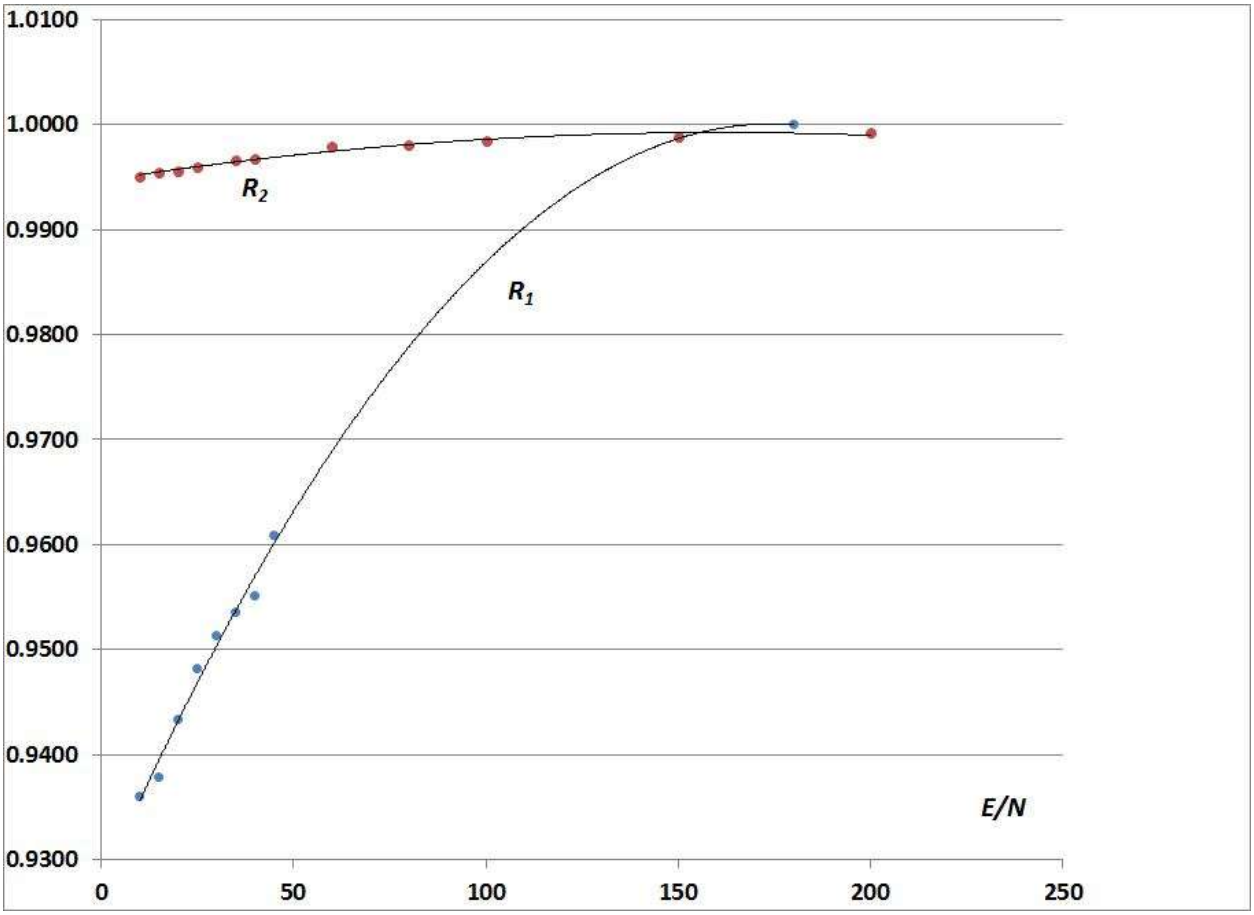

Fig. 5 of Viehland et al.

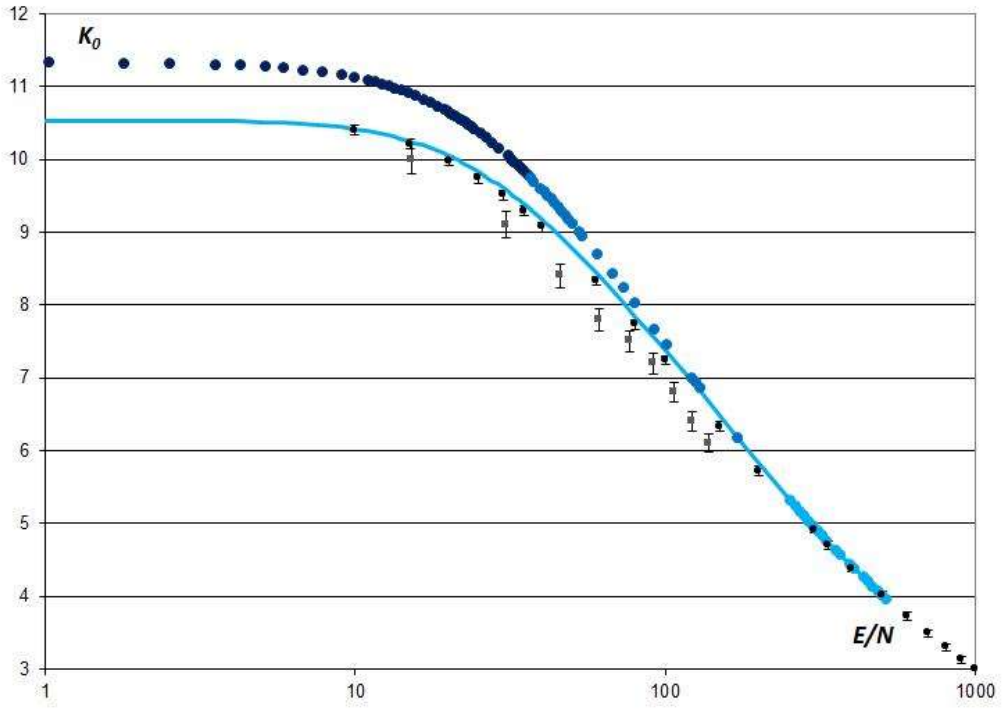

Fig. 6 of Viehland et al.

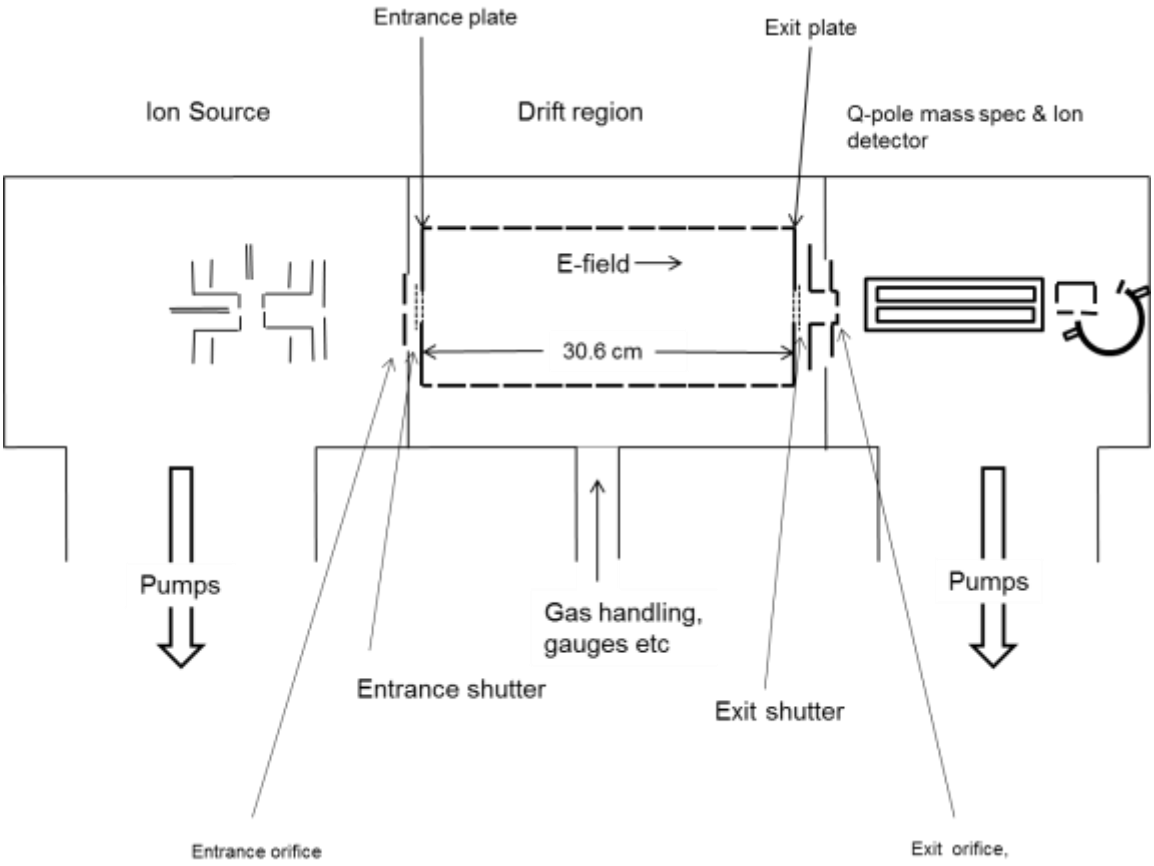

Fig. 7 of Viehland et al.

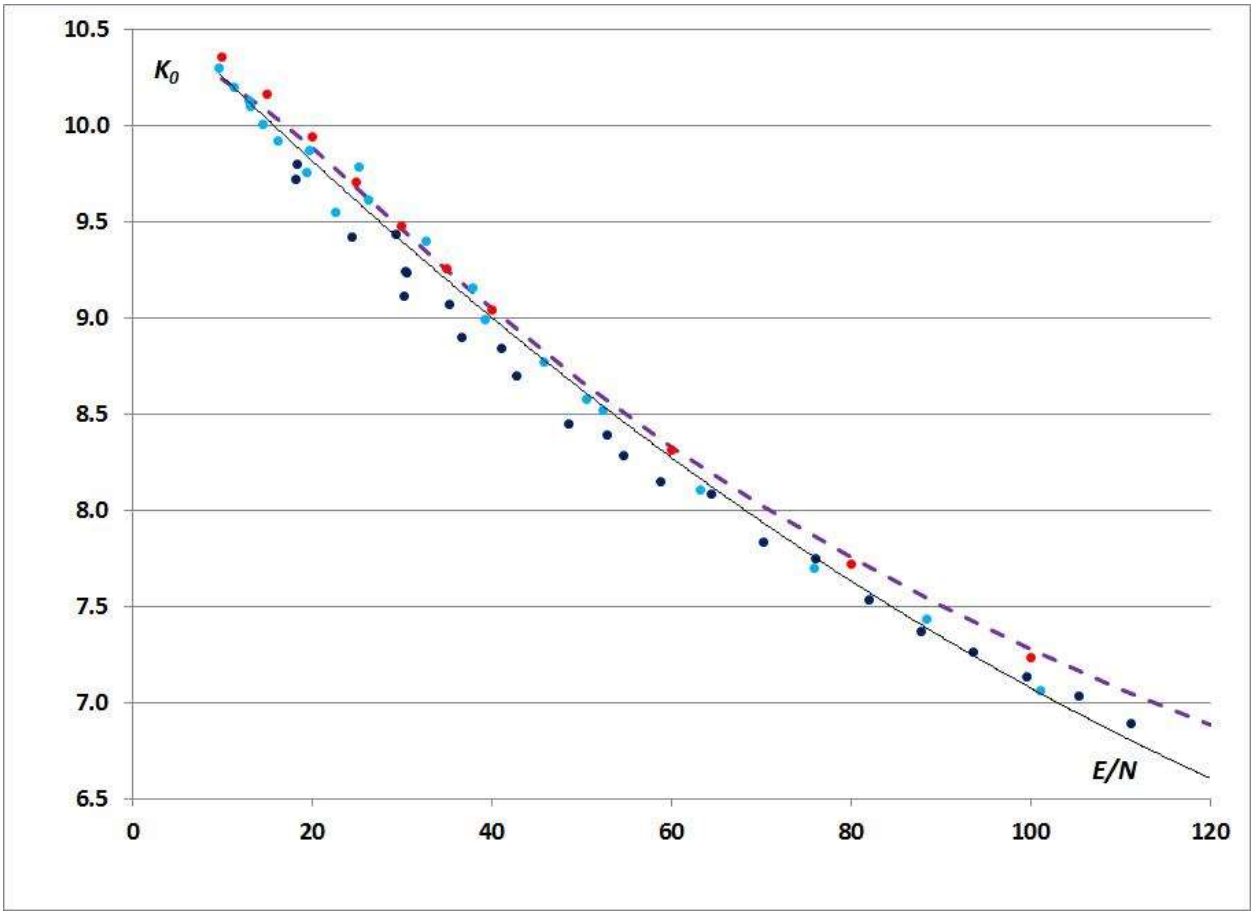

Fig. 8 of Viehland et al.

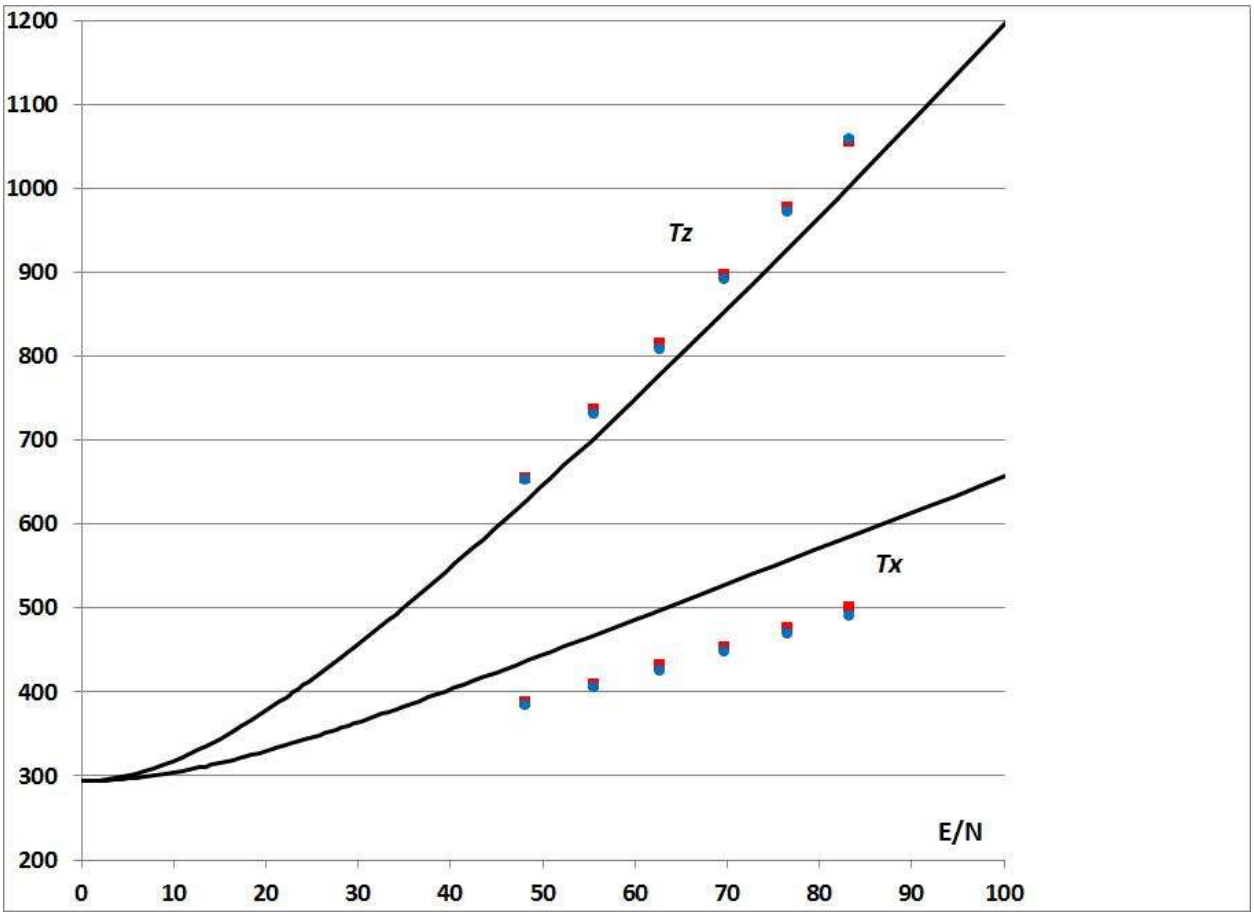

Fig. 9 of Viehland et al.

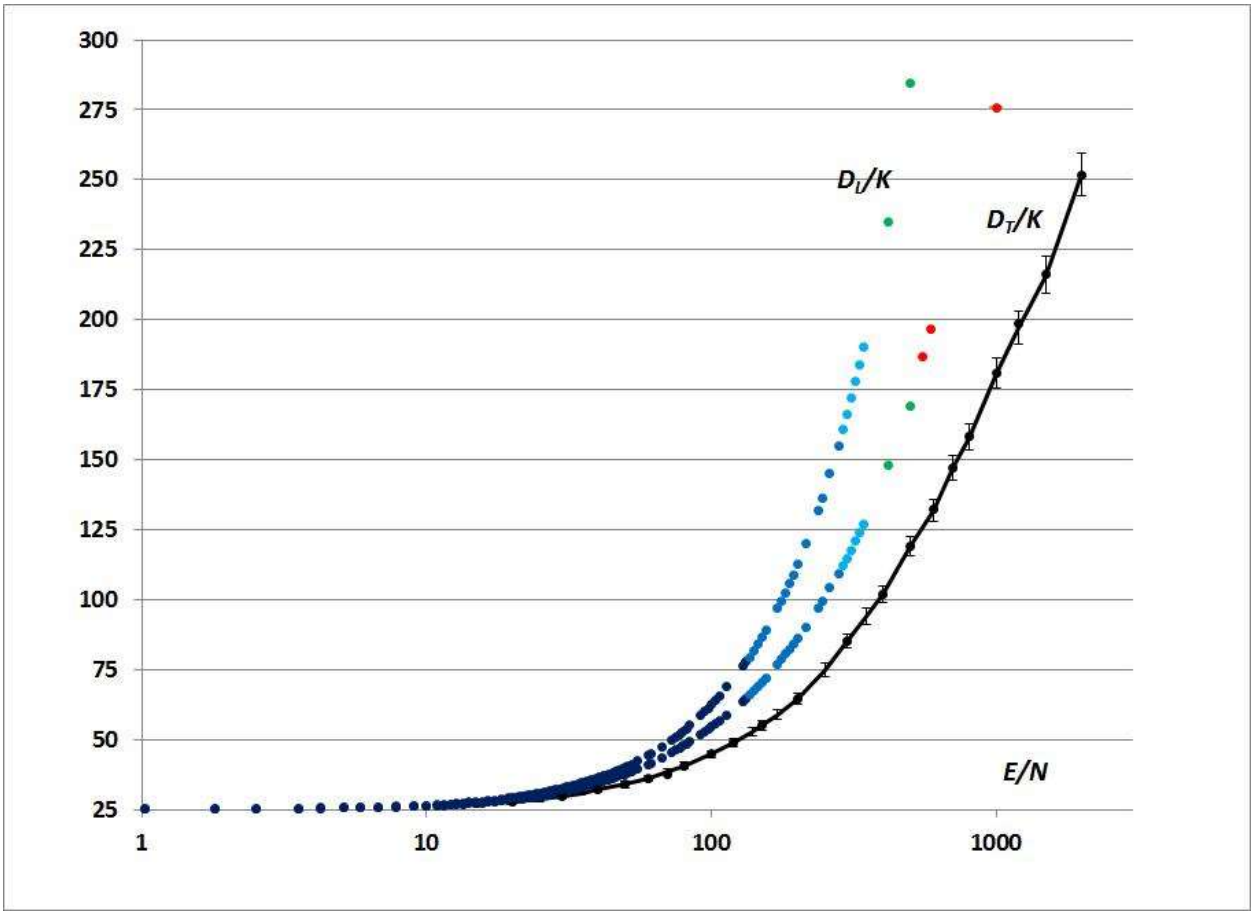

Fig. 10 of Viehland et al.

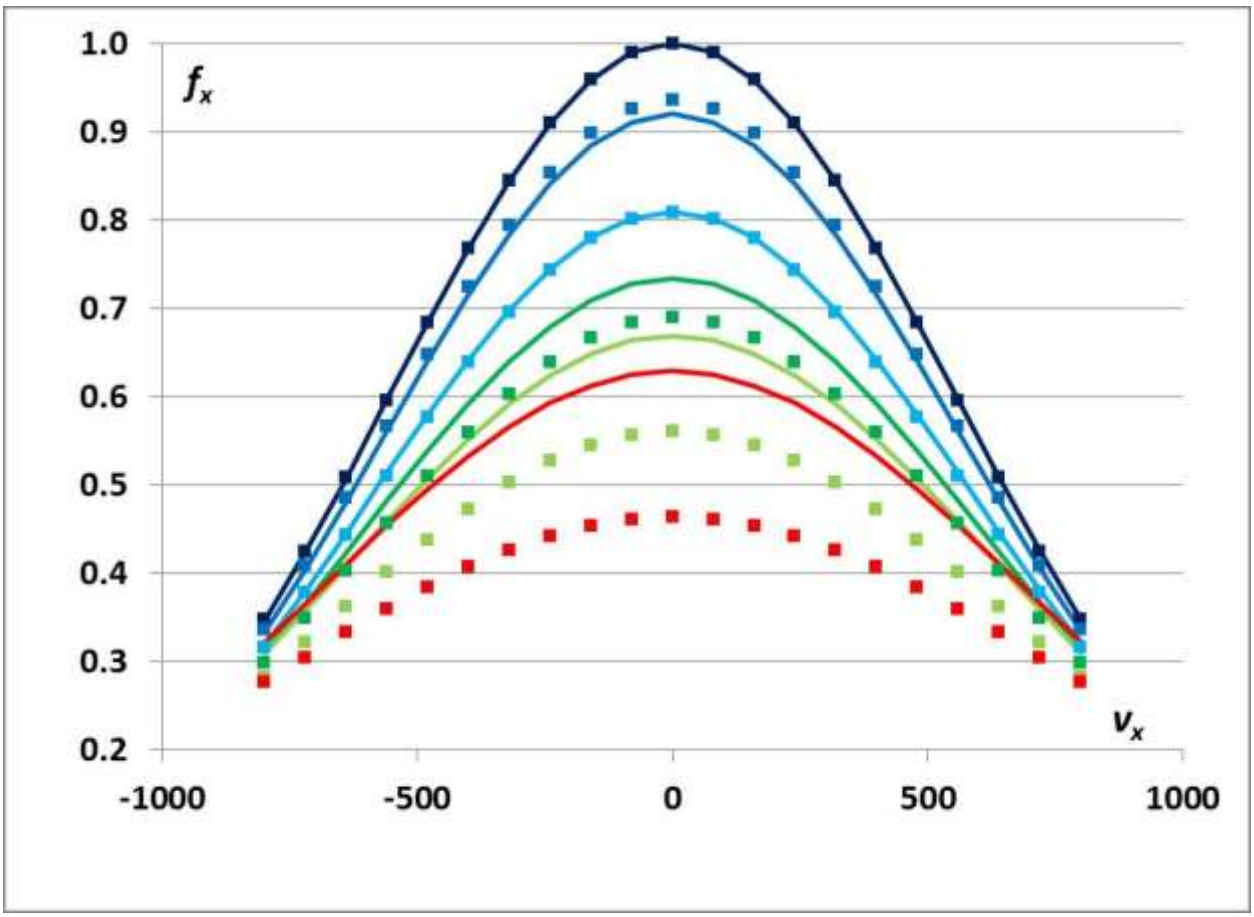

Fig. 11 of Viehland et al.

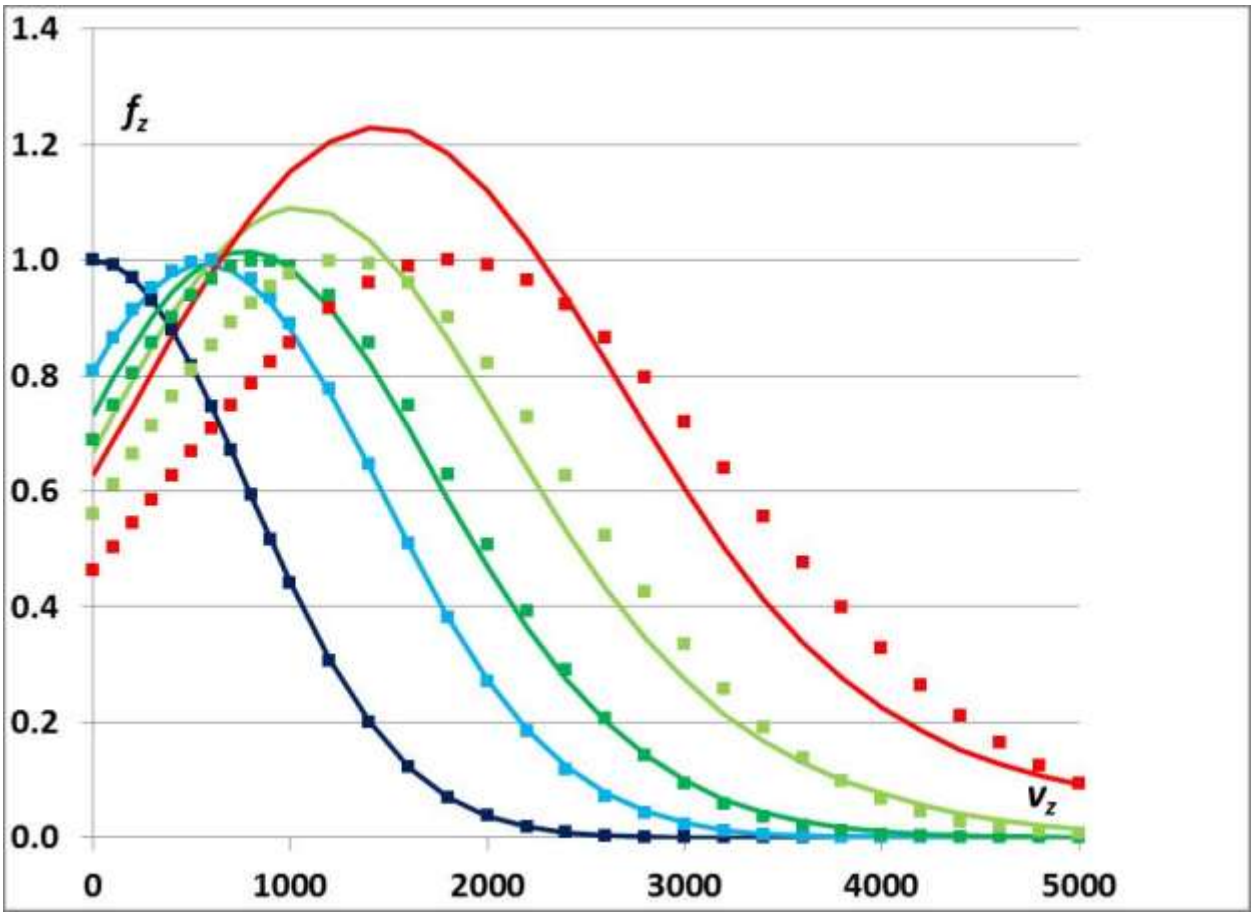

Fig. 12 of Viehland et al.

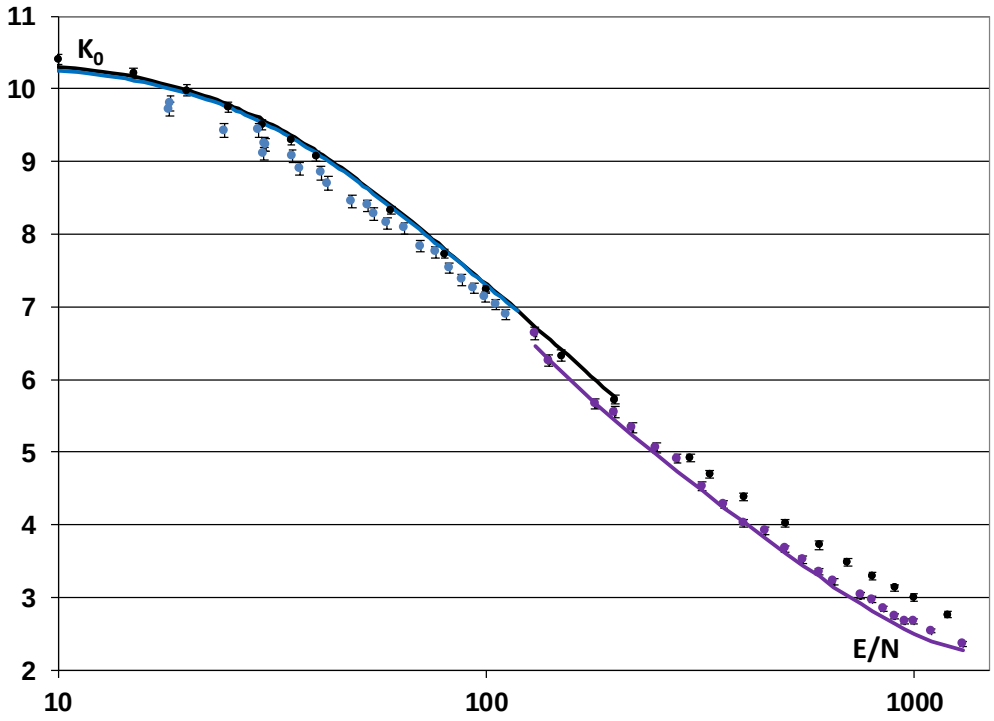

Fig. 13 of Viehland et al.